Volume 44 Number 4 September 1988

PHILIPS TECHNICAL REVIEW

Magnetic domains

Polyepoxides

Noise control

PHILIPS

Philips Technical Review (ISSN 0031-7926) is published by Philips Research Laboratories, Eindhoven, the Netherlands, and deals with the investigations, processes and products of the laboratories and other establishments that form part of or are associated with the Philips group of companies. In the articles the associated technical problems are treated along with their physical or chemical background. The Review covers a wide range of subjects, each article being intended not only for the specialist in the subject but also for the non-specialist reader with a general technical or scientific training.

The Review appears in English and Dutch editions; both are identical in contents. There are twelve numbers per volume, each of about 32 pages. An index is included with each volume and indexes covering ten volumes are published (the latest one was included in Volume 40, 1982).

PHILIPS TECHNICAL REVIEW

Volume 44, No. 4, September 1988

Contents

PHILIPS

PHILIPS TECHNICAL REVIEW

Volume 44, No. 4, September 1988

Magnetic domains in amorphous alloys for tape-recorder heads

H. J. de Wit and K. Jager

In modern video cassette recorders the magnetic material of the record/playback head is usually a ferrite. Ferrites are not so suitable, however, for the very high information densities necessary for recording on 8-mm tape, for example, and for digital video recording. For these applications certain amorphous cobalt-containing alloys are more promising. The magnetic behaviour of these materials is largely determined by the structure of the magnetic domains they contain. Scientists and engineers at Philips Research Laboratories have been studying ways of manipulating the domain structure to produce materials with the desired properties.

Introduction

Audio and video signals are usually recorded magnetically by drawing a tape coated with a magnetizable material past a magnetic head. The signal current generates a magnetic leakage field at the gap, and this field produces a particular magnetization in the tape. In 'axial' (or 'longitudinal') recording, which is the most common and the method we shall consider in this article, the magnetization in the tape has a preferred direction parallel to the tape surface; see *fig. 1*. The same head is generally used for playback, in which an electrical signal is induced in a coil in response to the magnetic flux from the tape, so that the recorded signal is reproduced.

A limitation on the density of the information recorded on the tape is the demagnetization due to adjacent domains magnetized in the opposite sense. The demagnetizing field should be no greater than the coercive field H_c, which is the minimum magnetic field-strength that reduces the induced magnetization to zero. As the domains become closer together, the demagnetization increases, so that the value of H_c (the coercivity) of the tape should be increased. Applications requiring very high information densities, such as video recording on 8-mm tape and digital video recording therefore require tapes with a very high coercivity (e.g. 100 kA/m). However, if such high-coercivity tapes are to be used, the magnetic material of the tape head must be of a higher quality [1].

To reverse the direction of magnetization in a tape the head must be capable of supplying a field of strength at least equal to the coercivity of the tape. This field depends on the magnetization M of the material. Frequently, however, the magnetic polarization J is considered rather than the magnetization. This is equal to $\mu_0 M$, where μ_0 is the permeability of free space. The maximum polarization, the 'saturation polarization' J_s of the head material, determines the maximum strength of the field produced by the head. With conventional ferrite heads J_s is about 0.5 T, not enough to reverse the magnetization in tapes with a coercivity of the

Dr H. J. de Wit and Ing. K. Jager are with Philips Research Laboratories, Eindhoven.

[1] J. P. M. Verbunt will discuss the manufacture of tape-recorder heads in a forthcoming issue of this journal.

order of 100 kA/m. Since the same head must also be suitable for reading the information on the tape, the head material must have a relative permeability μ_r that is sufficiently high at video frequencies (up to 5 MHz), e.g. $\mu_r > 1000$. Other requirements relate to the wear of the material and its magnetostriction, i.e. the change in length resulting from a change in magnetization.

To meet these requirements the use of certain cobalt-containing alloys has been proposed [2]. One suitable composition is $Co_{70.3}Fe_{4.7}Si_{15}B_{10}$. These alloys can be prepared in the form of an amorphous ribbon ('metallic glass'), produced by quenching a melt of the required composition by spraying it on to a spinning metal wheel. Thin amorphous films can also be deposited on a substrate by sputtering. The use of amorphous ribbons or sputtered thin films makes it possible to minimize the eddy currents always encountered in metallic materials. The alloys are soft magnetic materials, which means that they have a high permeability. They also have a high saturation polarization, and their magnetostriction can be kept very low with a material of appropriate composition. The requirement of a high permeability in the video frequency range can also be satisfied, but this does necessitate special precautions. These amount to 'engineering' the structure of the 'Weiss domains', the magnetic domains of different directions of magnetization found in ferromagnetic materials. The Weiss domains are separated by 'Bloch walls', in which the magnetization gradually changes from the direction in one domain to that in the neighbouring domain.

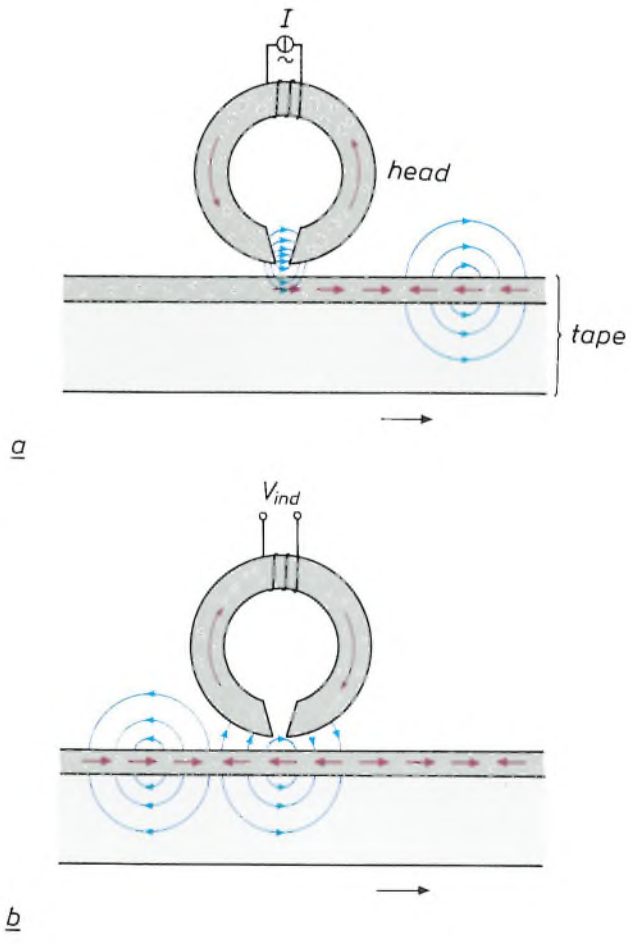

Fig. 1. *a*) Diagram representing longitudinal magnetic recording with a tape-recorder head on a moving tape coated with a magnetizable material. Magnetization directions in the materials are denoted by red arrows; magnetic lines of force outside them are denoted in blue. The signal current I generates a magnetic leakage field in the head gap via the magnetization of the head material. This leakage field records the signal on the tape by magnetizing the coating parallel to the surface of the tape. *b*) The recorded information is read with the same head. The magnetic flux from the tape magnetizes the head material, which induces a signal voltage V_{ind} in the coil in the head.

Soft magnetic materials, which are used for example in transformers, are in general characterized by the presence of large domains with walls that can readily be displaced by weak magnetic fields. For alternating magnetic fields with frequencies in the MHz range the wall velocity is generally too low to give a sufficiently high permeability. This can be substantially improved, however, if the alloy is made less magnetically soft by giving it a preferred direction of magnetization. One way of doing this is to anneal the material in a magnetic field. With this 'induced magnetic anisotropy', the positions of the domain walls and the size of the domains can be controlled in such a way that the magnetization takes place through simultaneous rotations of the magnetic moments in the domains, without the domain walls having to change position. These rotations are fast enough to give the material the required high permeability at high frequencies.

In the work described in this article a study was made of the way in which the induced magnetic anisotropy affects the domain structure and hence the magnetic properties, especially the permeability. Various cobalt-containing alloys were made in the form of amorphous ribbons or sputtered thin films [3]. The materials were annealed at different temperatures and in different orientations of the magnetic field. The domains were made visible with a polarizing microscope by means of the Kerr effect, i.e. using the change in the direction of polarization of polarized light on reflection from a ferromagnetic material, an effect that depends on the local direction of magnetization. The magnetic properties were determined in static magnetic fields and in alternating magnetic fields of different frequencies [4].

It was found that the direction of the magnetic field during annealing has a very marked effect on the domain structure [5]. The resultant domain structures

and their effect on the magnetic properties can now be explained reasonably well. In amorphous ribbons that are annealed with the magnetic field perpendicular to the axis of the ribbon the magnetization changes only through rotations of the magnetic moments. A high permeability can be obtained with such ribbons even at frequencies in the MHz range.

In this article we first describe the various domain structures that have been found in amorphous ribbons. Next we examine the magnetic behaviour of these ribbons in relation to their domain structures. Finally, we deal briefly with the changes in the magnetic properties of amorphous ribbons and sputtered thin films as a function of composition.

Control of the domain structure

Fig. 2 shows the domain structure of three amorphous ribbons 14 μm thick and about 1 cm wide, which were annealed at 300 °C in a magnetic field H_a in three different directions. The photomicrographs were made at $H = 0$, after saturating the ribbons with a magnetic field H in the longitudinal direction, i.e. parallel to the axis of the ribbon. In the ribbon annealed in a longitudinal field H_a, all the domains have '180° walls': the magnetic moments differ by 180° on opposite sides of the wall. The walls are parallel to H_a; the distance between them is about 0.4 mm. The ribbon that was annealed in a transverse field H_a, i.e. with the field perpendicular to the axis and parallel to the plane of the ribbon, also has 180° walls parallel to H_a. In this case the distance between the walls is about 0.2 mm. After an anneal with H_a perpendicular to the plane of the ribbon, a structure is found with a pattern in the form of a fine mesh; the domains are then no wider than about 3.6 μm. From the change in the Kerr effect when the ribbon is rotated with respect to the incident light beam it can be shown that the magnetization in these domains is perpendicular to the domain walls.

In the latter case a remarkable effect is observed when the ribbon is subjected to a magnetic field H whose orientation is opposite to that of the field at the original saturation. The magnetization inside the do-

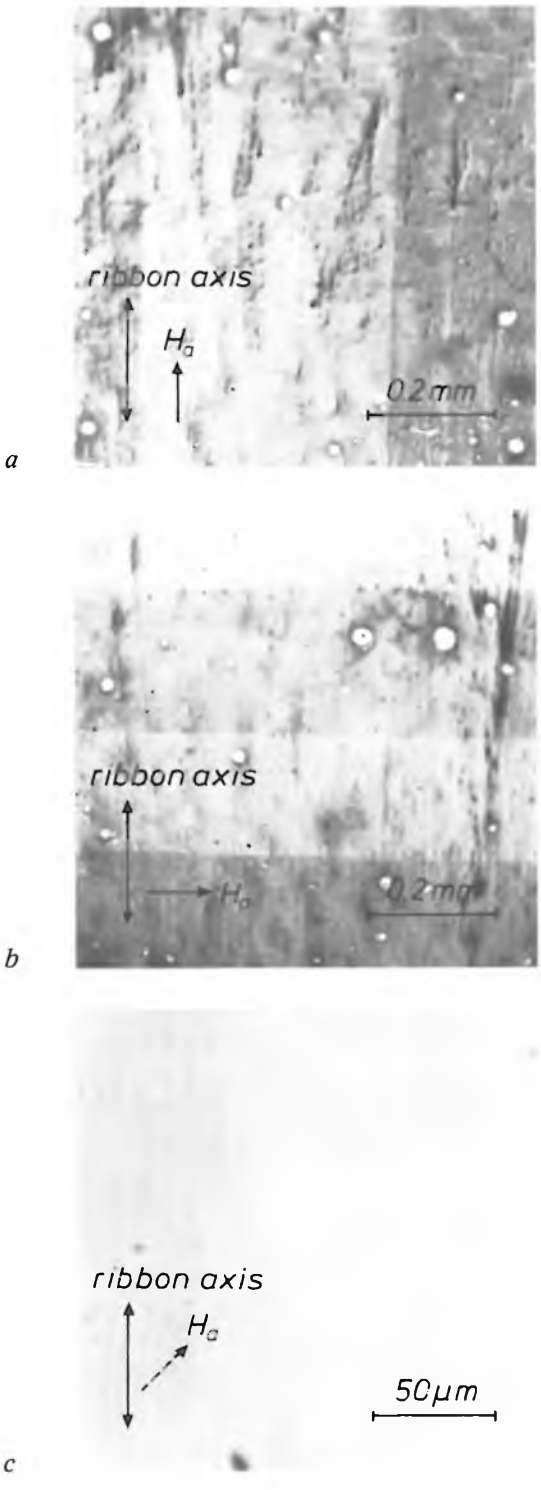

Fig. 2. Micrographs made with a polarizing microscope of domain structures in an amorphous ribbon (14 μm thick, 1 cm wide) of $Co_{70.3}Fe_{4.7}Si_{15}B_{10}$ after annealing at 300 °C in a magnetic field H_a for three different directions. The Kerr effect has been used to make the domains visible as light and dark bands. Other contrasts are due to surface unevenness. *a*) With H_a (1 kA/m) parallel to the axis of the ribbon, domains are formed whose walls are about 0.4 mm apart and parallel to H_a. *b*) With H_a (75 kA/m) perpendicular to the axis and parallel to the plane of the ribbon, domains are again formed with walls parallel to H_a, but now about 0.2 mm apart. *c*) With H_a (1200 kA/m) perpendicular to the plane of the ribbon a mesh pattern is formed; the distance between the domain walls is then about 3.6 μm.

[2] The possibility of using amorphous cobalt-containing alloys for tape-recorder heads was first reported by Japanese researchers in the early eighties.

[3] The amorphous ribbons were made by Ing. H. H. Stel, the sputtered thin films by A. W. A. Bakens, Ing. H. H. Stel and Ing. J. A. M. Tolboom.

[4] Experimental work on the amorphous ribbons was also performed by Ing. A. J. C. van der Borst and Ing. G. W. Turk. The investigation of the sputtered thin films was carried out in close cooperation with Ir F. W. A. Dirne and C. H. M. Witmer; some of the magnetic measurements were performed by Ing. P. Lasinski.

[5] H. J. de Wit and M. Brouha, Domain patterns and high-frequency magnetic properties of amorphous metal ribbons, J. Appl. Phys. 57, 3560-3562, 1985.

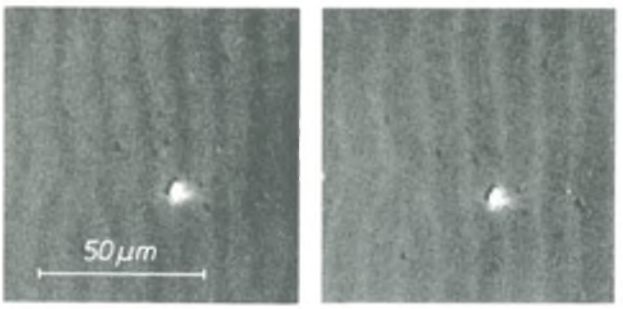

Fig. 3. Micrographs made with a polarizing microscope of an amorphous ribbon of $Co_{70.3}Fe_{4.7}Si_{15}B_{10}$ 29 μm thick and annealed in a magnetic field perpendicular to the plane of the ribbon at 200 °C. *a*) After magnetization parallel to the ribbon axis. *b*) After applying a magnetic field in the opposite direction and stronger than the coercive field. The resulting structures are complementary.

mains then reverses its direction as soon as the field H becomes stronger than the coercivity H_c of the material. This can be seen from a comparison of the micrographs before and after H_c is exceeded; see *fig. 3*. A light domain changes into a dark domain and vice versa.

The domain structure after an anneal in a magnetic field perpendicular to the plane of the ribbon can be described with the well-known model [6] shown schematically in *fig. 4*. According to this model the bulk of the material contains domains with 180° walls parallel to H_a. At the surface, however, 'flux-closure domains' arise, i.e. domains that form a closed magnetic flux with the domains in the bulk of the material. This results in surface domains in which the direction of magnetization is perpendicular to the domain walls. In this case the walls are parallel to the ribbon axis.

The formation of flux-closure domains occurs because it gives a reduction in the total magnetic energy density. The magnetostatic energy resulting from the emergent magnetic flux is then eliminated, and for homogeneous magnetization with a saturation polarization J_s this amounts to a reduction of the energy density by $J_s^2/2\mu_0$. For a material with $J_s = 1$ T this gives a value of 4×10^5 J/m^3. This is more than three orders of magnitude greater than the energy densities in the domain walls and in the flux-closure domains.

The width of the flux-closure domains is determined by the competition between the magnetic anisotropy energy in the flux-closure domains and the energy of the 180° walls. A high anisotropy energy in the flux-closure domains implies that a great deal of energy is necessary to rotate the magnetic moments away from their preferred direction, so that narrow domains are preferentially formed. If the energy of the 180° walls is high, however, it becomes energetically advantageous for wide flux-closure domains to form. If σ_w is the wall energy per unit area (J/m^2), D the thickness of the ribbon and K the anisotropy constant (J/m^3), then the width of the flux-closure domains is given by:

$$d = (2\sigma_w D/K)^{\frac{1}{2}}. \qquad (1)$$

The value of σ_w is determined by the anisotropy con-

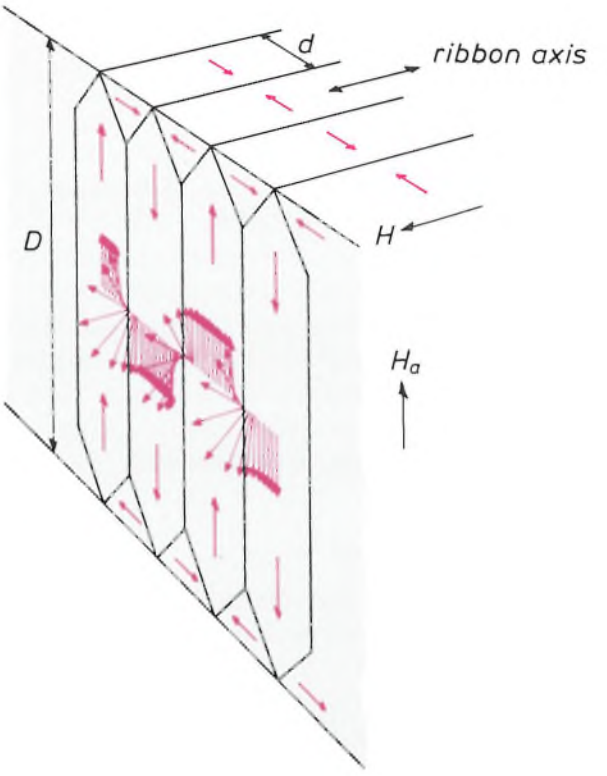

Fig. 4. Model explaining the domain structure in a ribbon of thickness D that has been annealed in a magnetic field H_a perpendicular to the plane of the ribbon and then magnetized with the magnetic field H along the ribbon axis. The red arrows indicate the direction of magnetization at $H = 0$. In the walls between neighbouring domains there is a gradual transition of the magnetization direction. At the surface there are flux-closure domains (of width d) in which the magnetization is perpendicular to the domain walls.

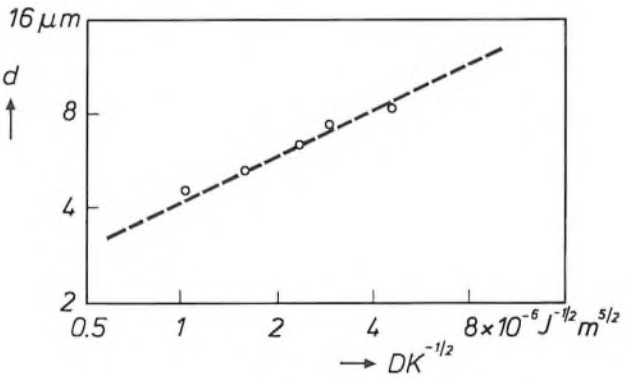

Fig. 5. Variation of the width of the flux-closure domains in an amorphous ribbon of $Co_{70.3}Fe_{4.7}Si_{15}B_{10}$ that has been annealed in a magnetic field perpendicular to the plane of the ribbon. The width d is shown as a log-log plot against $DK^{-\frac{1}{2}}$, where D is the ribbon thickness and K the anisotropy constant. The measured points lie on a straight line with a slope of 0.5.

stant and by the 'exchange' interaction that tries to make adjacent magnetic moments parallel:

$$\sigma_w = 4(AK)^{\frac{1}{2}}, \quad (2)$$

where A is the exchange constant (J/m). Substitution in eq. (1) then gives:

$$d = (8\,A^{\frac{1}{2}}DK^{-\frac{1}{2}})^{\frac{1}{2}}. \quad (3)$$

Fig. 5 shows a log-log plot of the measured width of the flux-closure domains against $DK^{-\frac{1}{2}}$. The measured points lie on a straight line with a slope of 0.5, in agreement with the relation that follows from eq. (3):

$$\log d = \tfrac{1}{2}\log 8A^{\frac{1}{2}} + \tfrac{1}{2}\log DK^{-\frac{1}{2}}. \quad (4)$$

The value of the exchange constant that can be derived from the straight line in fig. 5, $A = 4.9 \times 10^{-12}$ J/m, is comparable with the values reported for other similar materials [7].

Our results indicate that the model with flux-closure domains gives a reasonable explanation of the observed domain structure. It can also explain the reversal of the directions of magnetization in the domain for an increasing magnetic field in the opposite direction (fig. 3). Under the influence of this field the magnetic moments in the flux-closure domains tend to align themselves towards the magnetic field. This can be seen as an attempt to form domains with 360° walls: adjacent domains acquire the same direction of magnetization, while they are separated by walls with different directions of magnetization. When the magnetic field has reached a strength corresponding to the coercivity of the material, however, this becomes energetically so unfavourable that the direction of magnetization in all the domains reverses.

Effect on the magnetic properties

The three ribbons whose domain structures are given in fig. 2 show striking differences in their magnetic behaviour. In *fig. 6* the 'static' magnetization curves for these ribbons are plotted for a longitudinal magnetic field H. The ribbon annealed with a longitudinal magnetic field H_a gives a curve with a very steep central portion. This means that the permeability is very high: a weak magnetic field H is sufficient to cause very strong magnetization. This is typical of a magnetization process that comes about mainly through displacements of the domain walls, where the domains with the same direction of magnetization as the applied field grow at the expense of the domains with the magnetization direction in the opposite direction. The magnetization curve shows virtually no hysteresis; the displacement of a domain wall is a reversible process.

The ribbon annealed with a transverse field H_a also gives a curve with no significant hysteresis. The permeability, however, is now much lower. This indicates

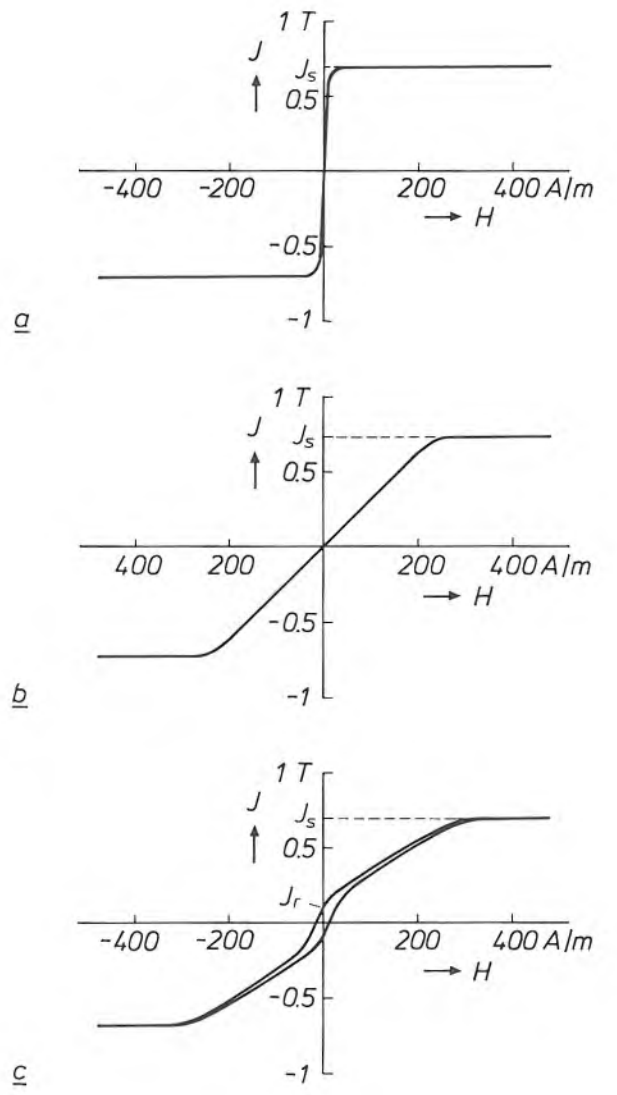

Fig. 6. 'Static' magnetization curves for the three ribbons in fig. 2, annealed in a magnetic field H_a in three different directions. The magnetic polarization J is plotted against the longitudinal magnetic field H, i.e. parallel to the ribbon axis. J_s saturation polarization. *a*) The ribbon annealed in a longitudinal magnetic field gives a curve with a very steep central portion, with virtually no hysteresis. *b*) The ribbon annealed in a transverse magnetic field gives a curve with a less steep central portion, again with virtually no hysteresis. *c*) The ribbon annealed in a magnetic field perpendicular to the plane of the ribbon gives a curve with an even less steep central portion and indicating distinct hysteresis. The remanence J_r is also shown for this case.

[6] This model was first described by L. Landau and E. Lifshitz, On the theory of the dispersion of magnetic permeability in ferromagnetic bodies, Phys. Z. Sowjetunion **8**, 153-169, 1935. Further work on the model was done by C. Kittel, Physical theory of ferromagnetic domains, Rev. Mod. Phys. **21**, 541-583, 1949.
See also the review article by C. Kittel and J. K. Galt, Ferromagnetic domains, Solid State Physics, part 3, Academic Press, New York 1956, pp. 437-564.

[7] H. Kronmüller, M. Fähnle, M. Domann, H. Grimm, R. Grimm and B. Gröger, Magnetic properties of amorphous ferromagnetic alloys, J. Magn. & Magn. Mater. **13**, 53-70, 1979.

that it is not the wall displacements that are important now, but the rotations of the magnetic moments towards the external field H.

The ribbon annealed with the field H_a perpendicular to the plane of the ribbon gives an even lower permeability. Here again the magnetization is determined mainly by the rotations of the magnetic moments. Unlike the other two cases, however, there is now a distinct hysteresis. This is attributable to a change in the mesh pattern. The hysteresis is related to the occurrence of remanence, i.e. the residual magnetization when the magnetic field is reduced from saturation to $H = 0$. The remanence can easily be explained from the model in fig. 4: after saturation and the return to $H = 0$, the magnetization in the domain walls still has a component in the direction of the original magnetic field.

The hysteresis found after annealing in a magnetic field perpendicular to the plane of the ribbon depends on the annealing temperature and the ribbon thickness. Some magnetization curves for different annealing temperatures and ribbon thicknesses are shown in *fig. 7*. When the annealing temperature is increased the central portions of the curves become less steep. The reduction in the permeability is due to the increase in the magnetic anisotropy. The remanence decreases at higher annealing temperatures and with thicker ribbons. This is in agreement with the domain-structure model. This model indicates that the ratio of the remanence J_r to the saturation polarization J_s will be approximately equal to the ratio of the width δ of the domain walls to the width d of the domains. The width of the walls is given by $\delta = \pi A^{\frac{1}{2}} K^{-\frac{1}{2}}$ [8] and the width of the domains is given by eq. (3). It follows from this that

$$J_r/J_s \approx \frac{\pi A^{\frac{1}{2}} K^{-\frac{1}{4}}}{(8D)^{\frac{1}{2}}}. \qquad (5)$$

The reduction in J_r at higher annealing temperatures can be attributed to the stronger magnetic anisotropy, i.e. to the higher value of K. The lower J_r found with a higher ribbon thickness D is also explained by this equation. Calculations for different values of K and D, with the value of A derived from fig. 5, give J_r/J_s-values that are about half those of the experimental values. A possible explanation for this is that the magnetization in the flux-closure domains also continues to have a component in the original direction of the magnetic field.

An important property for application in tape-recorder heads is the permeability in alternating magnetic fields, especially at high frequencies ($\geq$ 1 MHz). The frequency-dependence of the permeability, measured at a field amplitude of 5 A/m, is shown in *fig. 8* for the three ribbons of fig. 2. The ribbon annealed in a longitudinal magnetic field H_a gives by far the highest permeability at low frequencies (10 kHz). At higher frequencies, however, there is a very marked decrease. This is characteristic of magnetizations due to domain-wall displacements: the wall displacements are too slow to follow the magnetic field at high frequencies. In the other two cases the permeability is fairly constant up to about 1 MHz. The magnetization here is produced by rotations of the magnetic moments, which do take place fast enough to follow the magnetic field. The decrease in the permeability at frequencies in the MHz range can be attributed to eddy currents. Since the material is an electrical conductor, a rapidly varying magnetic field produces circulating currents. These produce a magnetic field in the opposite sense to the external field. As a result this field does not penetrate so far into the bulk of the material, so that the changes in magnetization are smaller.

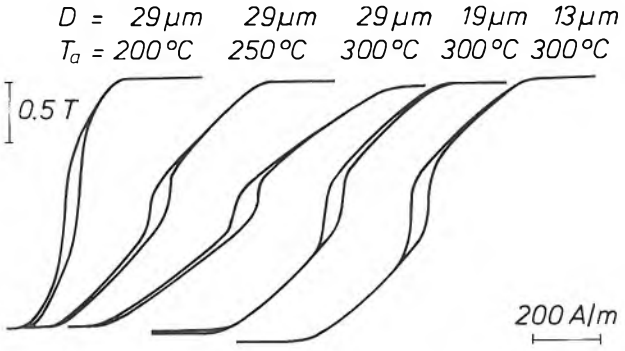

Fig. 7. Magnetization curves for an alternating magnetic field at a frequency of 1.3 Hz, measured for amorphous ribbons of thickness D annealed in a magnetic field perpendicular to the plane of the ribbon at a temperature T_a. An increase in T_a results in a curve with a less steep central portion and a lower remanence. Reducing D gives a higher remanence.

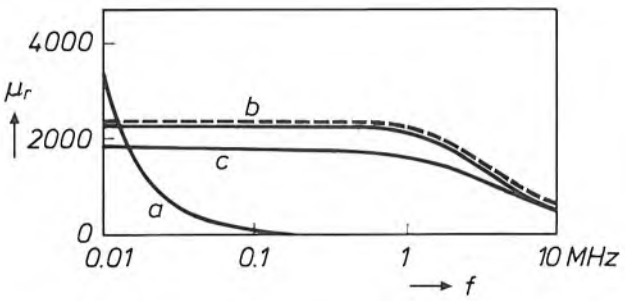

Fig. 8. Relative permeability μ_r as a function of frequency f for the three ribbons in fig. 2. The ribbon annealed in a longitudinal magnetic field (curve *a*) has a very high permeability at low frequencies; above 0.01 MHz, however, the permeability decreases sharply. The ribbon annealed in a transverse magnetic field (curve *b*) has a permeability that is constant up to about 1 MHz, then decreases. The measured curve agrees well with a calculation (dashed line) in which it was assumed that the magnetization is due to rotations of the magnetic moments in the domains, and that otherwise only eddy currents are involved. The ribbon annealed in a magnetic field perpendicular to the plane of the ribbon (curve *c*) has a somewhat lower constant μ_r up to about 1 MHz; again there is a decrease at higher frequencies.

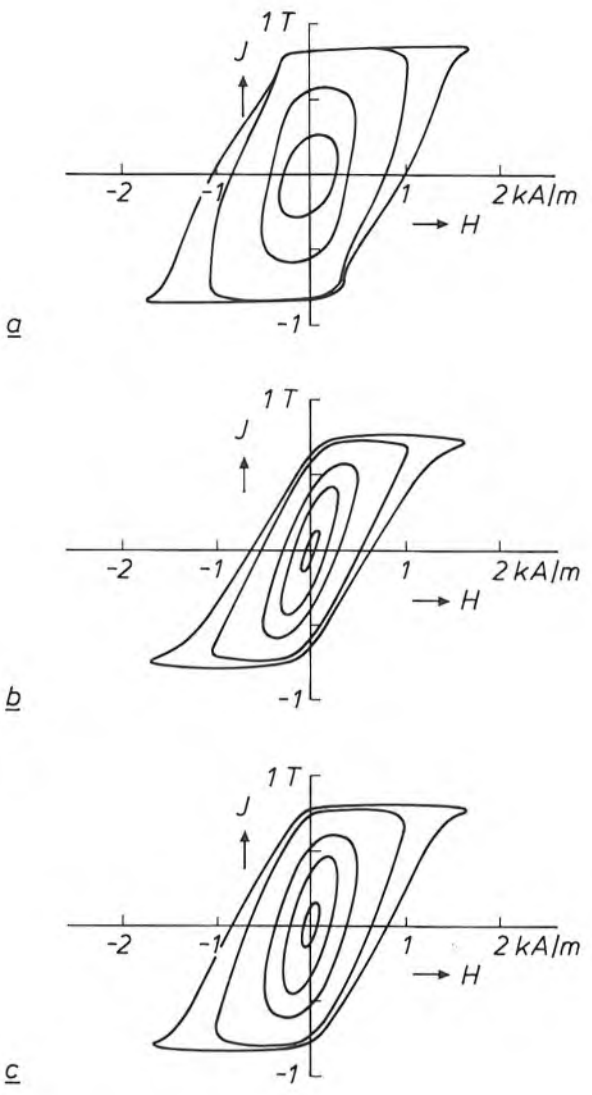

Fig. 9. Hysteresis loops for an alternating magnetic field at a frequency of 4.6 MHz for the three ribbons in fig. 2. Annealing in a longitudinal magnetic field (*a*) gives much broader loops than annealing in a transverse magnetic field (*b*) and in a magnetic field perpendicular to the plane of the ribbon (*c*). In (*c*) the loops are again broader than in (*b*).

The effect of eddy currents on the permeability has also been calculated[5] for the ribbon annealed in a transverse magnetic field (curve *b* of fig. 8). It was assumed in these calculations that the magnetization is entirely due to uniform rotations, corresponding to a static magnetization curve with a constant slope and virtually no hysteresis (fig. 6*b*). It was also assumed that there are no other losses. The frequency-dependence of the permeability can then be calculated exactly[9]. The result, which is also shown in fig. 8, is in very good agreement with the experimentally determined frequency-dependence of the permeability. This indicates that the assumptions about the rotation of the magnetic moments and the eddy currents are correct.

[8] See for example S. Chikazumi, Physics of magnetism, Wiley, New York 1964.

[9] See for example E. Olsen, Applied magnetism, a study in quantities, N.V. Philips Gloeilampenfabrieken, Eindhoven 1966, pp. 41-46.

At high frequencies all three ribbons give hysteresis loops that are wide compared with the static magnetization curves. *Fig. 9* shows a few loops measured at a frequency of 4.6 MHz. Here again the difference between wall displacements and rotations is clearly apparent. In the first case, strong fields are required to move the walls through the material, and therefore the loops in fig. 9*a* are distinctly wider than those in fig. 9*b* and *c*. The loops in fig. 9*c* are wider than those in fig. 9*b* because of the greater hysteresis in the static magnetization curve (fig. 6).

Composition-dependent changes in magnetic properties

With applications in tape-recorder heads in mind we investigated two kinds of alloy. One is formed by the amorphous ribbons discussed above, consisting of alloys of Co, Fe, Si and B. The magnetostriction of these materials can be made negligibly small by using the appropriate ratio of Co to Fe. The other kind comprises amorphous alloys of Co, Nb and Zr that are sputtered on a glass substrate. Here the magnetostriction can be suppressed via the ratio of Nb to Zr.

Besides the magnetostriction, the induced magnetic anisotropy is also an important property in the search for the most suitable composition. As we have shown, this largely determines the domain structure, which has a particularly important effect on the frequency-dependence of the permeability. The requirement for a high saturation polarization also has to be met, of course. We have investigated these properties in both of the alloys mentioned, not only varying the ratios of the different elements but also adding small amounts (about 2 at.%) of other elements. Some results of this investigation will now be briefly discussed.

Magnetostriction

We determined the magnetostriction λ_s of the ribbons by measuring the anisotropy constant K with and without a tensile stress σ. For a difference ΔK the value of λ_s is given by [8]:

$$\lambda_s = \tfrac{2}{3}\Delta K/\sigma. \qquad (6)$$

Immediately after manufacture, i.e. before annealing, an amorphous ribbon with a composition $Co_{70.3}Fe_{4.7}Si_{15}B_{10}$ gives no measurable magnetostriction: $\lambda_s \approx 0$. This changes, however, when the ribbon is first annealed in a magnetic field to induce the required magnetic anisotropy. *Fig. 10* shows how the magnetostriction depends on temperature during annealing in a transverse magnetic field. After annealing at 300 °C (for example) the magnetostriction is no longer negligible: $\lambda_s \approx 3 \times 10^{-7}$. If a ribbon with

$\lambda_s \approx 0$ is to be obtained in this case, then the ratio of Co to Fe must be changed slightly to obtain the compositions $Co_{70.8}Fe_{4.2}Si_{15}B_{10}$.

Fig. 10 also shows the effect of the annealing temperature after the addition of other elements. The addition of Mn results in a substantial increase in λ_s, particularly at high annealing temperatures. The addition of Pt, on the other hand, results in a marked decrease in λ_s, while adding other elements (Nb, Ta or Cr) has relatively little effect. In general, λ_s increases with the annealing temperature up to a value between 300 and 350 °C. At even higher temperatures a decrease occurs, probably because the Curie point of these materials is then exceeded.

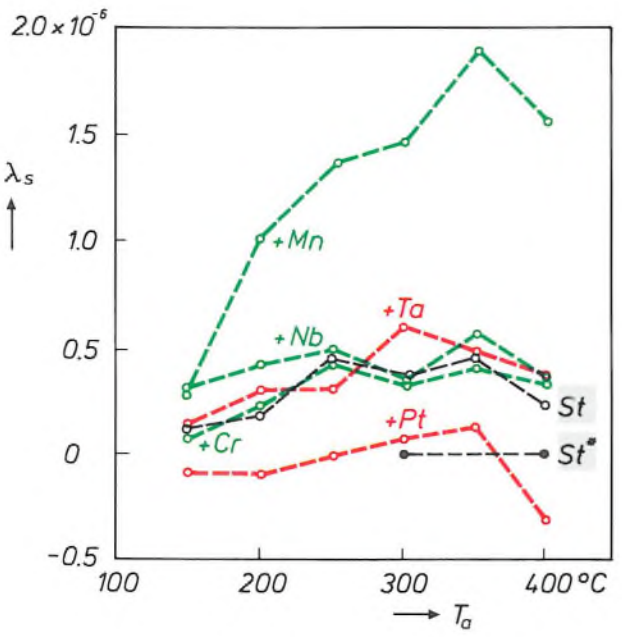

Fig. 10. The magnetostriction λ_s of some amorphous ribbons as a function of the temperature T_a at which they were annealed in a transverse magnetic field. Both for a ribbon with the 'standard composition' $Co_{70.3}Fe_{4.7}Si_{15}B_{10}$ (*St*) and for ribbons that also contain 2 at.% of Pt, Ta (red), Cr, Nb or Mn (green), the magnetostriction has its maximum value at an annealing temperature of 300 to 350 °C. The addition of Mn gives a much higher λ_s, the addition of Pt gives a very much lower value. To obtain $\lambda_s \approx 0$ at $T_a = 300$ °C the ratio of Co to Fe can also be modified to give the composition $Co_{70.8}Fe_{4.2}Si_{15}B_{10}$ (*St**).

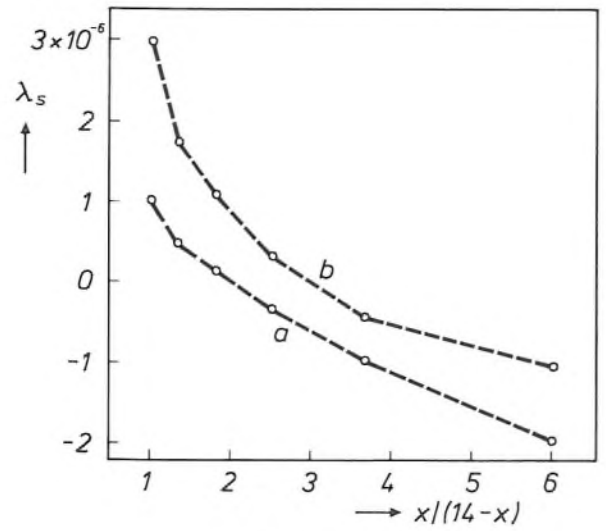

Fig. 11. The magnetostriction λ_s of sputtered thin films of the standard composition $Co_{86}Nb_xZr_{14-x}$ as a function of the ratio of Nb to Zr, without annealing (curve *a*) and after annealing in a transverse magnetic field at 390 °C (curve *b*). In both cases an increase in this ratio gives a decrease in λ_s. Annealing causes a positive shift in λ_s.

The magnetostriction of the thin films sputtered on a non-magnetic substrate was determined with an experimental arrangement designed at these Laboratories by M. Brouha. In this arrangement a specimen (i.e. substrate with magnetic layer) is placed in a magnetic field that rotates at a frequency of 5 Hz. One end of the specimen is fixed and the other is left free. The rotation of the field and the magnetostriction make the magnetic layer periodically change in length; this leads to curvature of the specimen and an excursion of the free end. The amplitude of this excursion is measured with a photosensitive sensor to an accuracy of better than 0.5 nm. The smallest value of the magnetostriction that can be measured with this arrangement is about 10^{-8}.

Annealing in a magnetic field also causes a change in the magnetostriction of thin films of alloys with Co, Nb and Zr. An example is shown in *fig. 11*. Here the measured magnetostriction is plotted against the ratio of Nb to Zr for non-annealed films and for films annealed at 390 °C in a transverse magnetic field. This anneal causes a positive shift in the values of λ_s. In this case λ_s is reduced to about zero when the composition is changed from $Co_{86}Nb_{9.3}Zr_{4.7}$ to $Co_{86}Nb_{10.5}Zr_{3.5}$.

Induced anisotropy and saturation polarization

The magnetic anisotropy induced in the amorphous ribbons that we investigated is generally significantly less than that in the sputtered films; see *fig. 12*. In both kinds of material the magnetic anisotropy constant K after annealing in a transverse magnetic field was found to be highest when the annealing temperature was in the region of 300 °C. The addition of another element (e.g. Ta) usually causes a slight decrease in K, but a 'magnetically active' element like Pt gives a marked increase. The explanation of these effects will not be considered here.

The effect of the composition on the saturation polarization J_s and the anisotropy constant K is shown in *fig. 13* for a large number of ribbons and sputtered films that were annealed at 300 °C in a transverse magnetic field. A higher value of J_s is generally associated with a higher value of K. The relation between J_s and K is important because these are the quantities that to a first approximation determine the

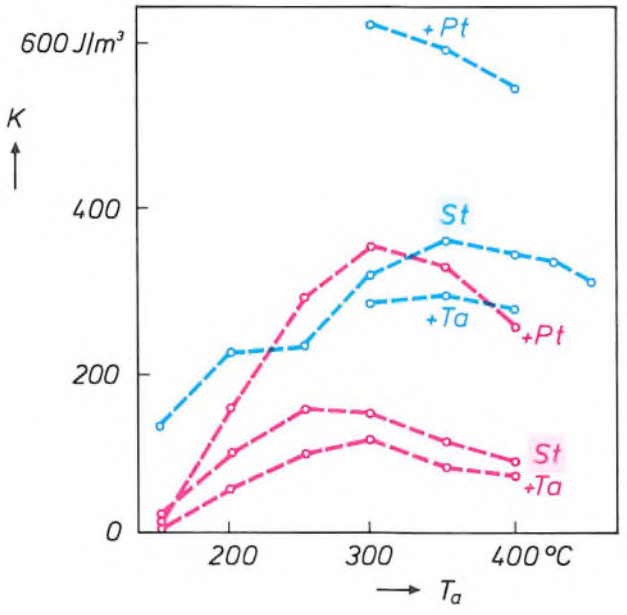

Fig. 12. The magnetic anisotropy constant K of amorphous ribbons (red) and sputtered thin films (blue), annealed in a transverse magnetic field, as a function of the annealing temperature T_a. The curves relate to the standard composition with no addition (*St*) and to this composition with 2 at.% of another element added. The highest K-values are reached with T_a at about 300 °C. The ribbon with the standard composition $Co_{70.3}Fe_{4.7}Si_{15}B_{10}$ has a much lower K-value at all annealing temperatures than the sputtered films with the standard composition $Co_{87.3}Nb_{8.8}Zr_{3.9}$. In both cases the addition of Ta gives a slight decrease in K, and the addition of Pt gives a marked increase.

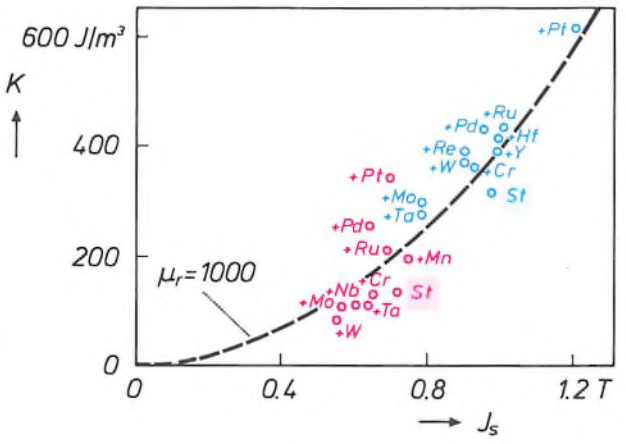

Fig. 13. The magnetic anisotropy constant K as a function of the saturation polarization J_s for amorphous ribbons (red) with the standard composition $Co_{70.3}Fe_{4.7}S_{15}B_{10}$ and with the addition of 2 at.% of another element, and for sputtered thin films (blue) with the standard composition $Co_{87.3}Nb_{8.8}Zr_{3.9}$ and with the addition of 2 at.% of another element. The materials were annealed at 300 °C in a transverse magnetic field. The dashed line corresponds to eq. (7), with $\mu_r = 1000$. Most measured points lie on or near this line. The sputtered films generally show not only a higher anisotropy but also a substantially higher saturation polarization than the ribbons. The additive that gives the strongest effect is Pt.

relative permeability μ_r of the material:

$$\mu_r = \frac{J_s^2}{2\mu_0 K}. \qquad (7)$$

The curve that corresponds to this equation for $\mu_r = 1000$ is also shown in fig. 13. For measured points below this curve the value of μ_r is greater than 1000, whereas the points above it correspond to smaller values of μ_r. In the ribbons the addition of most elements results in a distinct decrease in J_s: the effect on K is of minor significance, however. The addition of Pt, on the other hand, has a much stronger effect on K than on J_s. The sputtered films have a higher saturation polarization than the ribbons, and in most cases their anisotropy is also larger. The highest values of J_s and K were obtained with films containing Pt.

Summary. Certain amorphous cobalt-containing alloys with high saturation polarizations (about 1 T) show promise for applications in tape-recorder heads for video recording at high information densities. The relative permeability μ_r, which has to be very high ($\mu_r \gg 1000$) for reproducing the stored information, is largely determined by the structure of the magnetic domains. This can be controlled by annealing the alloys in a magnetic field, thus inducing a magnetic anisotropy. The effect on the permeability and the other magnetic properties depends on the direction of the magnetic field and the temperature during annealing, on the form of the material — spun ribbon or sputtered thin film — and on the precise composition.

Polyepoxides; formation and properties of their network structure

E. W. Meijer

Polyepoxides are polymer materials widely used in the electronics industry, and there is much interest today in a better understanding of their structure at the molecular level. The article below discusses two methods — phosphorescence spectroscopy and nuclear magnetic resonance spectroscopy — that can be used to give 'a closer view' of polyepoxides.

Linear-chain polymerization

Polyepoxides are obtained by the polymerization of epoxide monomers [1]. Epoxides have the structural feature of a three-membered ring, consisting of two carbon atoms and one oxygen atom. The simplest monomer is ethylene oxide:

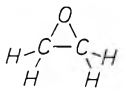

The ideal bond angles of carbon and oxygen cannot be realized in a three-membered ring. The bonds in an epoxide ring are forced to take up 'unusual' angles averaging 60° (instead of about 109°), which results in a structure possessing an internal ring strain and a corresponding strain energy of about 60 kJ/mol.

A chemical reaction that opens the epoxide ring (*fig. 1*) gives a gain in energy because of the loss of ring strain. This energy gain provides the thermodynamic basis for the 'ring-opening polymerization' of epoxides [2].

Apart from the fulfilment of this thermodynamic condition, a good kinetic route has to be found along which the polymerization can take place sufficiently rapidly. This usually requires a catalyst or initiator. By a catalyst we mean a compound that greatly increases the rate of polymerization but is not used up in the reaction. An initiator may be necessary to start the polymerization in some cases, but does take part in the reaction, usually becoming incorporated in the polymer.

Dr E. W. Meijer is with Philips Research Laboratories, Eindhoven.

Various monomers are of importance in the applications of epoxide-based polymers. In these complex monomers one or more hydrogen atoms in ethylene oxide are replaced by other atoms or groups of atoms. Steric interaction between these substituents in the epoxide ring increases the ring strain. However, this may not give an increased reactivity in polymerizations; this depends on the nature of the reaction mechanisms for the various types of polymerization.

The polymerization can take place in the form of an addition reaction between compounds of the same kind, 'chain polymerization', or in the form of a step reaction — a succession of individually catalysed reactions between different kinds of compounds — 'condensation polymerization' [2].

Chain polymerizations can be initiated by activating the epoxide ring of a monomer by a catalyst in such a way that it can react with a non-activated monomer. The resultant dimer remains activated, and so do the trimer, tetramer and so on. In this way hundreds or thousands of monomers can be concatenated to form a polymer in the 'propagation step' of the polymerization. In a 'termination reaction' the chain is deactivated and the catalyst is re-formed. It can then be used again to catalyse the formation of another chain. The catalyst can be an acid (a cationic catalyst) or a base (an anionic catalyst). *Fig. 2a* shows the progress of an acid-catalysed polymerization. The polymerization of epoxides started by an initiator can be regarded as a repetitive reaction in which the initiator is lengthened by one monomer unit at each repetition. The initiator may be for example an organo-

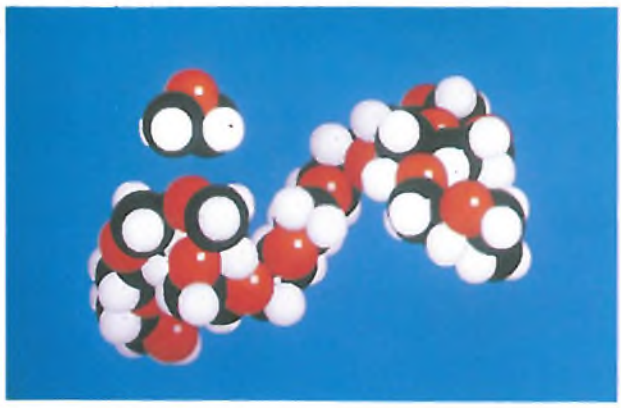

Fig. 1. Three-dimensional computer model of ethylene oxide (*a*) and polyethylene oxide (*b*). The spheres represent the Van der Waals radii of the various atoms. The models were produced by 'molecular-mechanics optimization'.

metallic compound (coordinative initiation). In this case the polymerization is terminated without the initiator being re-formed.

The reaction rates of these chain polymerizations may differ considerably. For instance, polymerizations catalysed by an acid like BF_3 may often have to be carried out at a temperature below $-50\,°C$ to sustain the reaction, which is exothermic. On the other hand, polymerizations catalysed by a base, such as imidazole, only reach an acceptable rate at a temperature of about 100 °C.

The second form of polymerization, condensation polymerization, is of great practical importance, since it is the basis for the widely used epoxy resins. Although it is mainly polymer networks that are produced in this way, the principle will be discussed here for linear chains. To synthesize such polymers a mixture of two kinds of compounds is used. One kind has two epoxide rings and the other contains two functional groups that can react with epoxide rings, e.g. amines, hydroxides or phenolic hydroxyl groups. Multiple repetition of the ring opening, catalysed each time, produces a polymer in a succession of steps (fig. 2*b*).

The macroscopic (physical, chemical and mechanical) properties of the polymeric end-product depend on the way in which the polymers are formed. In chain polymerization a cyclic ether (an epoxide) is converted into a linear — and much more stable — ether, built up by a regular repetition of a C-C-O unit in the main chain of the polymer (fig. 2*a*). Such regularly structured polymers have a strong tendency to crystallize. In condensation polymerizations of epoxides the main chain always contains polar side chains in the form of hydroxyl groups. These polymers are not so highly regular, and therefore tend to have the properties of amorphous glassy systems.

For completeness it should be mentioned that there are also combined forms of the two modes of polymerization described above, which can result in highly complicated systems.

Formation of three-dimensional networks

A recent article in this journal dealt with the applications of polymer chemistry in the electrical industry [3]. An important feature in this chemistry is making polymer material insoluble. This can be done by linking linear polymers together, or by simultaneously polymerizing and cross-linking multifunctional monomers [4]. The latter method is widely used for making polyepoxides from bisepoxides containing two epoxide rings. Some examples are shown in *fig. 3*.

The many and various ways in which the chemical structure of these bisepoxides can be modified, and the diversity in polymerization reactions, ensure that materials can be produced to fit the particular specifi-

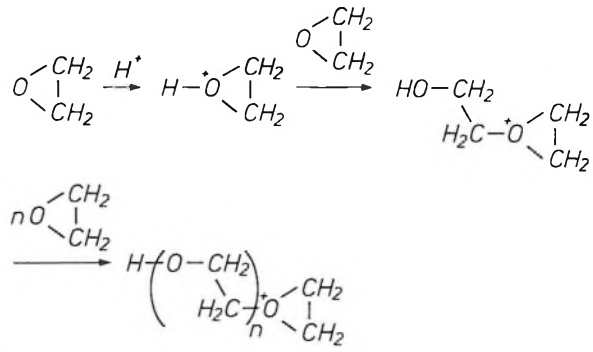

a

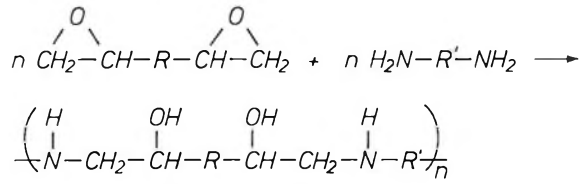

b

Fig. 2. *a*) Mechanism of an acid-catalysed chain polymerization of epoxides. *b*) Reactions for a condensation polymerization of a bisepoxide with a diamine. *R* and *R'* represent linking chains.

[1] Y. Ishii and S. Sakai, in: Ring-Opening Polymerization, K. C. Frisch and S. L. Reegen (eds), Marcel Dekker, New York 1969, pp. 13-109.

[2] S. Inoue and T. Aida, Cyclic ethers, in: Ring-Opening Polymerization, part 1, K. J. Ivin and T. Saegusa (eds), Elsevier, Barking 1984, pp. 185-298.

[3] L. K. H. van Beek, Polymer chemistry in the electrical industry, Philips Tech. Rev. 42, 149-159, 1986.

[4] J. G. Kloosterboer, G. J. M. Lippits and H. C. Meinders, Photopolymerizable lacquers for LaserVision video discs, Philips Tech. Rev. 40, 298-309, 1982.

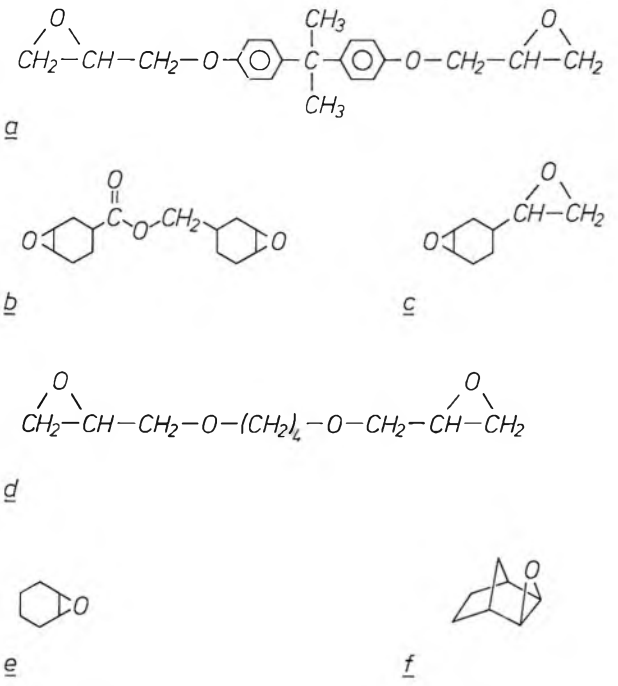

Fig. 3. Four examples of widely used bisepoxides and two monoepoxides that we used as models. *a*) bisphenol-A diglycidyl ether, *b*) (3,4-epoxycyclohexyl)-methyl 3′,4′-epoxycyclohexane carboxylate, *c*) 1-epoxyethyl-3,4-epoxycyclohexane, *d*) 1,4-butanediol-diglycidyl ether, *e*) cyclohexene oxide, *f*) exo-2,3-epoxynorbornane.

cations for any application. For most purposes condensation polymerization of two different compounds is used, because this is the method that offers the most variations in molecular structure. Examples are the epoxy resins for the encapsulations of ICs and discrete components, laminated resins for printed-circuit boards, and many adhesives, some of them conductive.

The formation of a three-dimensional network is described in this article by taking the chain polymerization of bisepoxides as an illustration. The illustration has more general validity, however. Polyepoxide networks are formed in a series of repeated reactions in which the low-viscosity bisepoxide is gradually converted into a hard end-product. This increase in viscosity during the reaction reduces the mobility of the monomers and their functional groups. The effect is intensified after the 'gel point' has been passed. The reduced mobility of the monomers and their functional groups has little influence, however, on the reaction rate of polymerization and cross-linking. Because the collisions between molecules become slower, fewer collisions are required on average to cause a reaction [5]. The rate of conversion is not in fact limited until 'vitrification' occurs. At this point the mobility of the functional groups that have not yet reacted is virtually zero because of the well-advanced cross-linking and the associated loss of free volume. In this 'glassy' state the reaction comes to a virtual standstill, without all the epoxides necessarily having reacted. The transition from the initial situation to the end-product is shown schematically in *fig. 4*.

In practice it is often advantageous if the polyepoxide networks are formed rapidly at the lowest possible temperature. Since this conflicts with other practical requirements — for durable and workable monomers without premature reaction — use is often made of 'latent catalysts'. In a latent catalysis an inert compound first has to be converted into a highly active catalyst before the polymerization can proceed. Latent catalysts can be formed by both thermal and photochemical methods.

Proper control of polymer formation requires not only a general understanding of what happens during the formation process but also a closer understanding of events on a molecular scale. Ultimately, local chemical variables determine the macroscopic physical and mechanical properties. It would be desirable to know the degree of homogeneity of the structure during the polymerization process, the precise reaction mechanisms in the different local situations, the probability of isomers being formed in the various mechanisms, and — not least — the ultimate mobility of individual polymer segments and the associated ultimate degree of conversion.

The insolubility of polymer networks makes it difficult to acquire this information, and in some cases even impossible. In the following sections two examples will be discussed that illustrate the way in which an investigation of this kind can be tackled.

Both examples deal with the formation and structure of polyepoxide networks, formed by chain polymerization with simultaneous cross-linking of bis-

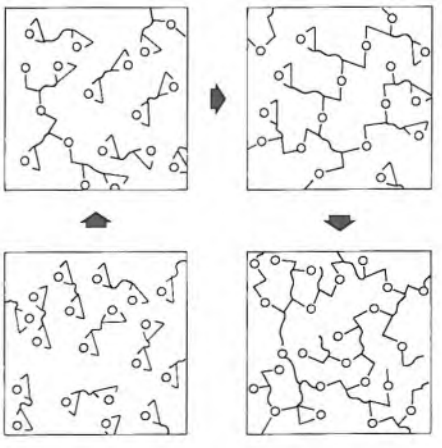

Fig. 4. Diagram of the formation of a polyepoxide network from a bisepoxide.

epoxides. In the first example the way the polymerization process takes place is broadly known and we can therefore concentrate on more detailed aspects, such as the molecular mobility. It will be shown how phosphorescence spectroscopy can be used to monitor the change in the molecular mobility of polymer segments during the formation of a network. If the mechanism of polymerization is entirely unknown, however, this must be established first. The second example will show how the mechanism of network formation for model compounds can be studied by means of nuclear-magnetic-resonance spectroscopy, a powerful method for the spectroscopic investigation of organic molecules [6].

Molecular mobility of polyepoxide networks [7]

Phosphorescence spectroscopy as an investigative method

A diaryl-iodonium compound can be used as the latent catalyst or photoinitiator for the formation of a polyepoxide network if the network is to be formed at room temperature while being exposed to light or other radiation (*fig. 5*) [8]. We have studied this network formation and the microstructure of the networks formed with the aid of phosphorescence spectroscopy, a method that has previously only been used in research on linear polymers.

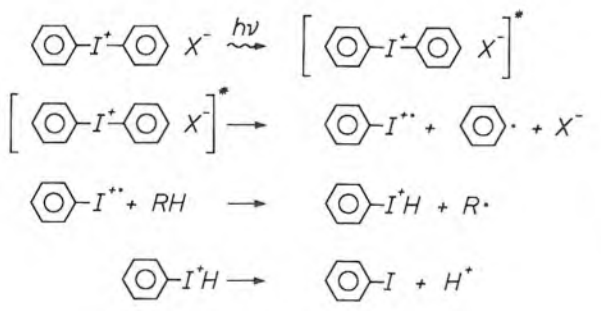

Fig. 5. The photochemical formation of an acid from a diaryl-iodonium salt[8], where X^- represents AsF_6^-, SbF_5^-, etc. In the first reaction step the diaryl-iodonium salt is brought into an excited state (*), which then decays into reactive particles, mainly cations (+), radicals (•) and radical cations (+ •).

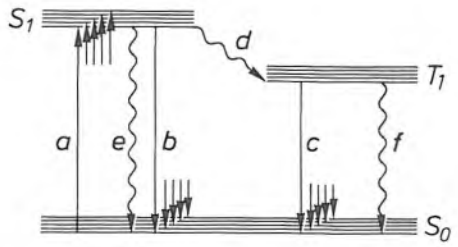

Fig. 6. Simplified representation of the Jablonski diagram for S_0, S_1 and T_1 of an organic compound. Absorption (*a*), fluorescence (*b*), phosphorescence (*c*), intersystem crossing (*d*) and non-radiative transitions (*e* and *f*) are represented. The small arrows indicate the fine structure of the vibration.

Since most organic compounds possess a singlet ground state S_0, the absorption and emission of light by these compounds can be represented in a simplified Jablonski diagram (*fig. 6*). In the case of phosphorescence the radiative transition takes place from an excited relatively long-lived triplet state (T_1). Its long lifetime makes this triplet state extremely sensitive to non-radiative decay, which can occur as a result of molecular vibrations or collisions with other molecules in a triplet state (e.g. oxygen molecules). To record phosphorescence spectra it is therefore always necessary to limit the molecular mobility as far as possible. One way of doing this is by performing the measurements at low temperatures on an amorphous glass in which the molecule of interest has been dissolved.

As noted in the introduction, during polymer formation the product gradually becomes more viscous. This means that its molecules become less mobile. In the cured network the molecular mobility is low but is still subject to temperature-dependent changes. In this stage the lifetime of the triplet state and the intensity of the phosphorescence can provide important information about dynamic changes in the network.

The half-life τ of the triplet state is given by:

$$\tau^{-1} = \tau_r^{-1} + \tau_{nr}^{-1},$$

where τ_r is the lifetime of the triplet state in the radiative decay and τ_{nr} is its lifetime in the non-radiative decay. The temperature dependences of intensity and

[5] P. J. Flory, Principles of Polymer Chemistry, Cornell University Press, Ithaca, N.Y., 1953, pp. 69-104.

[6] The following books should interest those who would like to know more about this subject;
on polymer chemistry:
G. Odian, Principles of Polymerization, 2nd edition, McGraw-Hill, New York 1981;
F. W. Billmeyer, Jr., Textbook of Polymer Science, Wiley Interscience, New York 1971;
D. W. van Krevelen, Properties of Polymers, Elsevier, Amsterdam 1976;
P. J. Flory, Principles of Polymer Chemistry, Cornell University Press, Ithaca, N.Y., 1953;
on photochemistry and photophysics:
J. E. Guillet, Polymer Photophysics and Photochemistry, Cambridge University Press, Cambridge 1985;
N. J. Turro, Modern Molecular Photochemistry, Benjamin/Cummings, Menlo Park, Cal., 1978;
on nuclear magnetic resonance spectroscopy for organic molecules:
H. Günther, NMR-Spectroskopie, Thieme Verlag, Stuttgart 1973;
J. B. Stothers, Carbon-13 NMR Spectroscopy, Academic Press, New York 1972.

[7] E. W. Meijer and R. J. M. Zwiers, in: Crosslinked Epoxies, B. Sedláček and J. Kahovec (eds), Walter de Gruyter, Berlin 1987, pp. 27-40.

[8] J. V. Crivello, Cationic polymerization — iodonium and sulfonium salt photoinitiators, Adv. Polym. Sci. 62, 1-48, 1984.

half-life are well known from work on linear polymers, and are given by [9]:

$$(I_f/I_p)(I_{p,0}/I_{f,0}) - 1 = A \exp(-E_a'/RT),$$
$$\tau^{-1} - \tau_0^{-1} = B \exp(-E_a''/RT),$$

where I_f, $I_{f,0}$, I_p and $I_{p,0}$ are respectively the intensities of the fluorescence at the temperatures T and $T = 0$, and of the phosphorescence at the temperatures T and $T = 0$. τ and τ_0 are the lifetimes at T and $T = 0$. A and B are constants; E_a' is the energy term denoting the temperature-dependence of the intensity of the phosphorescence and E_a'' is the energy term denoting the temperature dependence of its lifetime.

Fig. 7 shows emission characteristics of a polyepoxide network that we have studied. Intermediates that occur during the photoinitiated decomposition of the diaryl-iodonium compounds used as a latent catalyst are found to give rise to fluorescence with a maximum at a wavelength of 340 nm and to phosphorescence with a maximum at a wavelength of 480 nm (fig. 7*a*). The phosphorescence decays almost exponentially with a half-life of 1.6 s at room temperature (fig. 7*b*). In our investigations we used the diaryl-iodonium compound di(4-*tert*-butylphenyl)-iodonium-hexafluoroarsenate as latent catalyst and emission source. Although the nature of the emitting species has not been identified in detail, this is no objection to using the compound as a 'probe'.

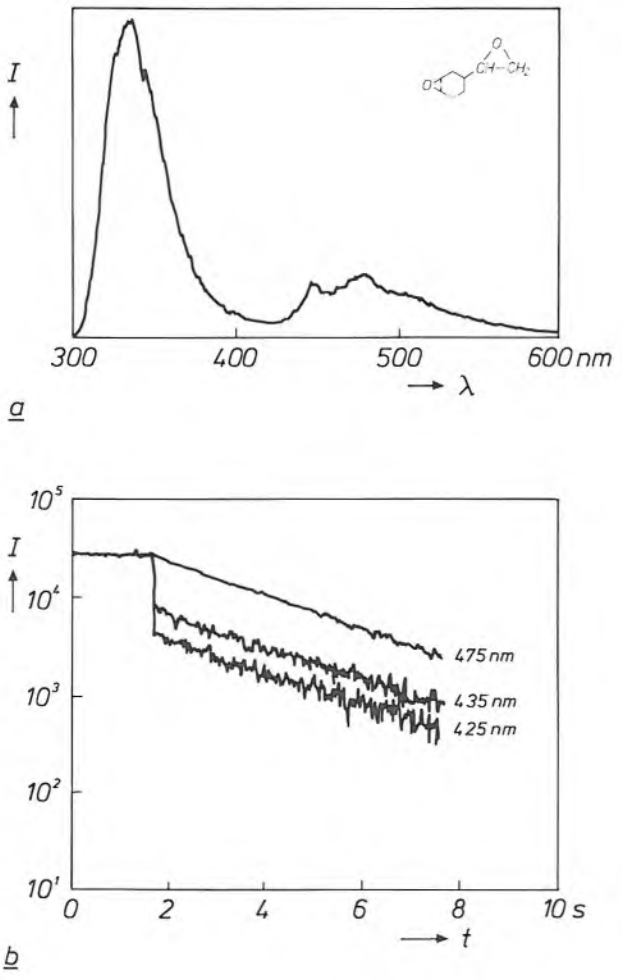

Fig. 7. *a*) The emission spectrum (intensity I against wavelength λ) of a network of 1-epoxyethyl-3,4-epoxycyclohexane (fig. 3*c*), recorded at an excitation wavelength of 254 nm at room temperature. *b*) The decay of the excited triplet state for the same network, detected at three different wavelengths indicated in the figure. The excitation wavelength was 290 nm.

Molecular mobility as a function of polymerization time [10]

If the fluorescence and phosphorescence intensities are measured as a function of the time in which the polymerization and cross-linking take place, an exponential increase is observed in both cases. The immediate rise in intensity of the fluorescence at the start of polymerization is followed, after an induction period dictated by the monomer used, by a rise in the intensity of the phosphorescence. In the case of the phosphorescence the induction period and the slope of the increase in intensity are interrelated (*fig. 8*).

As stated, all these effects are determined by the rate at which the molecular mobility in the continuously cross-linking polymer matrix is slowed down. This slowing down of the mobility is determined by the reaction rate of the polymerization and the change in viscosity on a micro-scale brought about by each step in the polymerization. It is the combination of these factors that interests the polymer chemist and can be investigated with this method of phosphorescence spectroscopy.

The end of the induction period indicates that the molecular mobility has reached a certain threshold value. The slope of the increase in phosphorescence is a measure of further changes in mobility.

Small variations in the composition of the original materials are found to give rise to changes in the polymerization processes that can readily be measured. *Fig. 9* shows the result of phosphorescence measurements on mixtures of 1-epoxyethyl-3,4-epoxycyclohexane and 1,4-butanediol-diglycidyl ether. The first bisepoxide has a rigid structure and reacts rapidly, whereas the second is flexible and reacts relatively slowly. This has the result that when the proportion of the flexible monomer in the original mixture increases, it takes longer for the molecular mobility to slow down sufficiently for phosphorescence to occur. This is reflected in a longer induction period and not so steep a rise in the intensity curve.

We have compared the results of this new method of studying the processes of polymerization and net-

work formation with results of microcalorimetric experiments (DSC for Differential Scanning Calorimetry) on the same epoxides. In these experiments we monitored the progress of the reaction by measuring the heat of reaction produced per unit time. A comparison of fig. 8 and *fig. 10* shows that both methods lead to corresponding conclusions: listing the various bisepoxides in order of polymerization rate as measured with the microcalorimeter gives exactly the same sequence as listing them in order of network formation as determined by phosphorescence spectroscopy.

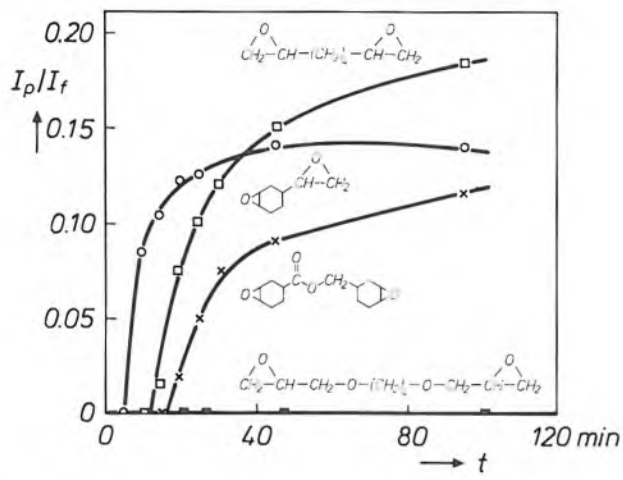

Fig. 8. Relative increase I_p/I_f in the phosphorescence intensity as a function of the polymerization time t for four polyepoxides at room temperature.

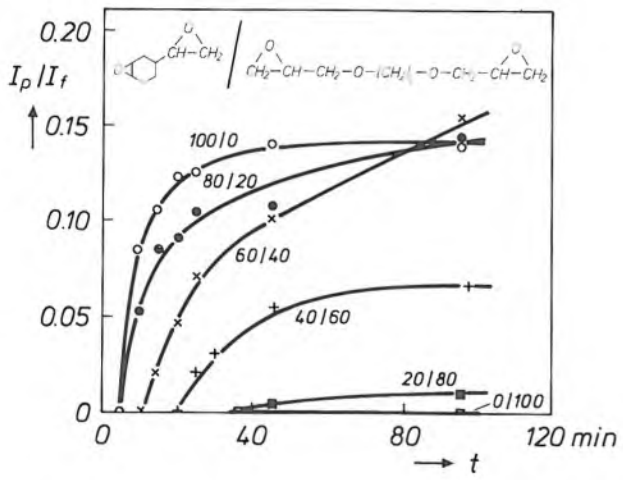

Fig. 9. As in fig. 8., for mixtures of two epoxides.

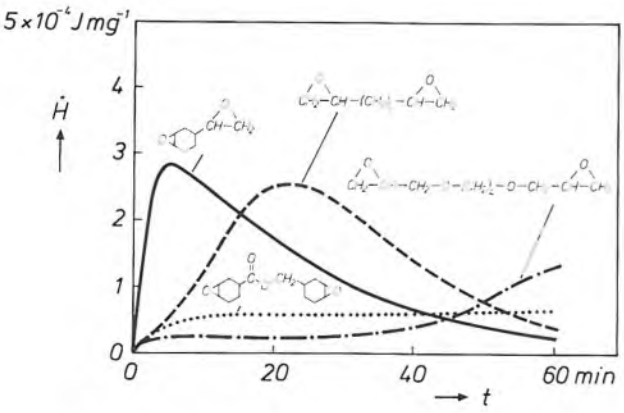

Fig. 10. Result of microcalorimetric (DSC) measurements on the photopolymerization of four bisepoxides at room temperature. The heat flux $\dot{H}$ is plotted as a function of the reaction time t.

The phosphorescence measurements had therefore taught us something about the rate of polymerization, but the method still had more to offer.

We also wanted to monitor the progress of the polymerization from measurements of the half-life of the excited triplet state. To determine this half-life we made a 'time-resolved' measurement of the phosphorescence. It was then found that the *half-life* of the triplet state is *not* dependent on the polymerization time, unlike the *intensity* of the phosphorescence, which does depend on the polymerization time. We assume that the explanation for this remarkable effect must reside in the inhomogeneous structural formation of the polyepoxide network. It seems to us that the increase in the degree of cross-linking does not take place homogeneously but is localized. This is to say that during the formation of the network the matrix consists of areas with a relatively high degree of conversion (giving phosphorescence with a long half-life) and areas with a relatively low degree of conversion (no phosphorescence). Extension of the regions with a high degree of conversion at the expense of areas with a low degree of conversion will then *increase* the intensity of the phosphorescence, but will not affect the half-life.

Other indications of the inhomogeneous polymerization postulated here have been found from electron-resonance-spectroscopy measurements on trapped free radicals in these polyepoxides [10]. Inhomogeneous polymerizations have also been postulated in other polymer networks [11].

Molecular mobility as a function of temperature [12]

As well as information about the rate of polymerization, phosphorescence spectroscopy can also provide information about dynamic-structural as-

[9] A. C. Somersall, E. Dan and J. E. Guillet, Photochemistry of ketone polymers XI, Macromolecules **7**, 233-244, 1974;
K. J. Smit, R. Sakurovs and K. P. Chiggino, Temperature dependence of fluorescence and phosphorescence from probe molecules in polymer substrates, Eur. Polym. J. **19**, 49-53, 1983.

[10] E. W. Meijer, D. M. de Leeuw, F. J. A. M. Greidanus and R. J. M. Zwiers, Molecular mobility studies in polyepoxides obtained by photoinitiated cationic polymerization, Polym. Commun. **26**, 45-47, 1985.

[11] J. G. Kloosterboer, Network formation by chain crosslinking photopolymerization and its applications in electronics, Adv. Polym. Sci. **84**, 1-61, 1988.

[12] E. W. Meijer and R. J. M. Zwiers, Molecular mobility of polyepoxide networks as revealed by emission spectroscopy and mechanical analysis, Macromolecules **20**, 332-338, 1987.

pects of the three-dimensional network ultimately formed. To obtain this information we measure the intensity of the phosphorescence and the lifetime of the triplet state as a function of temperature. This is illustrated by the results of measurements on the relatively flexible network of 1,4-butanediol-diglycidyl ether. At room temperature it will not normally be possible to produce phosphorescence from such a network, but by reducing the temperature the molecular mobility of the network can be reduced sufficiently for phosphorescence to occur (*fig. 11*).

The increase in the intensity of the phosphorescence and the lifetime of the associated triplet state when the temperature is reduced can most easily be investigated by plotting the measured values as Arrhenius curves (*fig. 12*). Both curves in the figure consist of

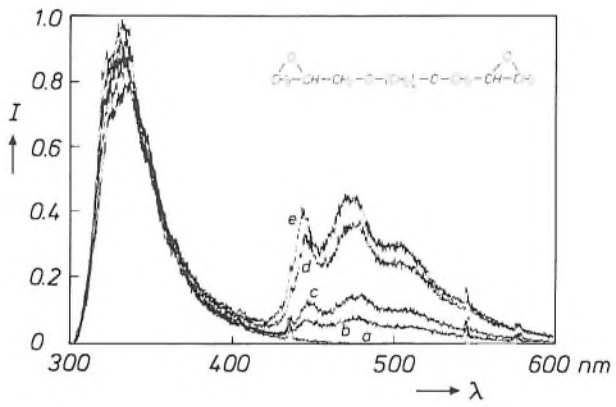

Fig. 11. Emission spectra of a network of 1,4-butanedioldiglycidyl ether (fig. 3*d*) for different temperatures at an excitation wavelength of 254 nm: *a*) 296 K, *b*) 279 K, *c*) 273 K, *d*) 233 K, *e*) 193 K.

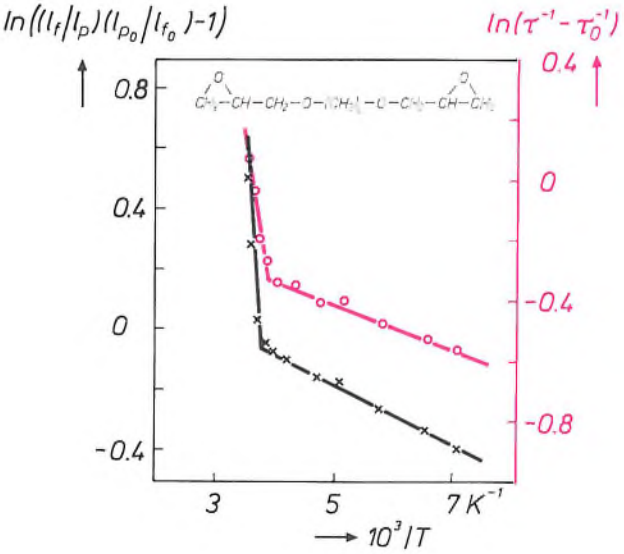

Fig. 12. Temperature dependence of the (relative) phosphorescence intensity (left) and of the (relative) half-life of the excited triplet state for a network of 1,4-butanediol diglycidyl ether (fig. 3*d*).

two linear sections with a sharp transition at a temperature of about 260 K. The slope of a straight section is a measure of the activation energy of the mobility (or microviscosity) in the network. The low-temperature section (with $E_a = 6$ to 8 kJ/mol) corresponds to a state of low mobility and therefore little non-radiative decay from the triplet state. The changes are mainly attributable to molecular vibrations and to local degrees of freedom in conformation. The high-temperature section corresponds to a state of greater mobility ($E_a \geqslant 150$ kJ/mol) and the radiative decay and the non-radiative decay of the triplet state take place at a comparable rate. Here *parts* of the macromolecule are able to move, culminating eventually in the macroscopic glass-rubber transition.

These Arrhenius curves are similar for all the polyepoxide networks that we have studied (*Table I*). The slopes of all the low-temperature sections are the same, and the transition to the high-temperature section is at about 260 K on all the curves; only the slopes of the high-temperature sections differ. It is only in these slopes that the considerable differences between the molecular structures of the initial monomers become apparent. And indeed they show that the mobilities of the networks built up from flexible molecules like 1,4-butanediol-diglycidyl ether have a higher activation energy than those of the networks built up from rigid molecules like 1-epoxyethyl-3,4-epoxycyclohexane.

When the polyepoxides mentioned above are subjected to DMTA measurements (dynamic mechanical thermal analysis) it is found that the polymers built up from flexible monomers have a narrow transition region at low temperatures, and that the polymers built up from rigid molecules have a broad transition region at higher temperatures.

A comparison of the phosphorescence measurements and the mechanical measurements reveals the following picture of the dynamic structure of polyepoxide networks. In all the polyepoxides that we have studied the molecular mobility at very low temperatures is the same below the threshold value. In all the polyepoxides the molecular mobility starts to change at the same temperature, about 260 K. The movements that then occur are related to the molecular mobility of the individual groups. In this part of the curve above 260 K we therefore see a premonition of the macroscopic glass-rubber transition state, which will appear for the most mobile network at the lowest temperature when the temperature is increased again.

This — non-destructive — method of phosphorescence spectroscopy therefore gives us valuable supplementary information about the microscopic structure of polymer networks and the complicated way in which they are formed.

Table I. Experimentally obtained values for the activation energies, determined from Arrhenius curves as shown in fig. 12. The columns E_{a_1} give the values in kJ/mol as determined for the low temperatures, and columns E_{a_2} give the values for the higher temperatures. The columns T give the transition temperature in K.

Polymer networks of the epoxides in fig. 3	Intensity			Half-life		
	E_{a_1}	T	E_{a_2}	E_{a_1}	T	E_{a_2}
c	8	259	14	3	240-250	9
d	8	262	170	6	263	115
c:*d* = 4:6	8	266	22	5	263	17
b	6	225-257	23	5	245-250	10
b:*e* = 1:1	4	259	42	3	259	14

Sometimes it will also be desirable to find out more about the particular local reaction mechanism for each polymerization step during the formation of a network. An investigation of this type that we performed with the aid of NMR spectroscopy is described in the next section.

A mechanism for epoxide polymerization

An investigation in which the mechanism of a promising new catalyst-initiator system for epoxide polymerization was studied [13] will now be described as our second example.

The high thermal and chemical stability of polyepoxide networks, combined with good electrical insulation, makes polyepoxides eminently suitable as encapsulating materials for electrical components. If these networks are to be produced by an ionic reaction mechanism, generally a very effective method, then it is particularly important that no ionogenic impurities such as catalysts should be left behind in the network. A likely material investigated for this purpose was tris(acetylacetonato) aluminium — referred to from now on as $Al(acac)_3$ — in combination with phenolic compounds. Nothing was previously known about the mechanism of the polymerization produced with this system.

NMR spectroscopy as an investigative method

The theoretical background of the nuclear-magnetic-resonance spectroscopy we used for this investigation has been dealt with several times in this journal [14], but with no particular attention to the opportunities offered by NMR spectroscopy for a better understanding of the structure of complicated organic compounds (including polymers). This form of spectroscopy can be used with particular advantage for studying the hydrogen atoms (with spin quantum number 1/2) in these compounds.

An external magnetic field causes the energy associated with a nuclear spin to 'degenerate' into two energy levels, one by aligning the nuclear spin with the field, and the other by aligning it in the opposite sense to the field. A resonance between these two levels gives rise to NMR signals. Because there are differences in the local magnetic field around a nuclear spin, due to the electron distribution in the molecule, the energy required for the resonance of each physically non-identical hydrogen atom does not have exactly the same value. These differences in resonance energy can be observed via the 'chemical shift' in the NMR spectrum, which is characteristic of the various substitution patterns in the molecule.

The spin-spin couplings that frequently occur have the effect of splitting the resonances, and are therefore an additional source of information. Spin-spin couplings in NMR spectroscopy arise from the splitting of energy levels of nuclear spins caused by the presence of adjacent spins (at a distance of up to about three covalent bonds). The parallel and antiparallel combinations cause the splitting. Identical spins do not split one another.

NMR spectroscopy can also identify other nuclei in much the same way as those of the hydrogen atoms. In organic chemistry NMR spectroscopy is very useful for studying ^{13}C atoms. The use of powerful magnetic fields (up to 13.8 Tesla), with high-resolution equipment and the application of various complicated pulse techniques, have meant that NMR spectroscopy has now become one of the most powerful spectroscopic methods for analysing organic molecules. The impressive results reported have included the explanation of the structure of extremely complex proteins and parts of DNA[15]. Polymers have also been the subject of extensive investigations with NMR[16].

Most information is now obtained from liquid systems, although solid-state NMR is in full development. We have investigated the mechanism of chain polymerization with the aid of a model compound, a monoepoxide. This forms soluble polymers, making high-resolution NMR possible.

[13] Contributions to this part of the investigation were made by F. W. v.d. Wey, J. P. H. Heynen, H. Draayer, A. W. de Bruyn, A. Schokker and C. Kruk.

[14] P. R. Locher, Proton NMR tomography, Philips Tech. Rev. **41**, 73-88, 1983/84.
D. J. Kroon, Nuclear magnetic resonance, Philips Tech. Rev. **21**, 286-299, 1959/60.

[15] R. Kaptein, S. Stob, R. M. Scheek, K. Dijkstra and T. W. Schleich, High-field and photo-CIDNP studies of biological molecules, Bull. Magn. Reson. 2, 28-31, 1981;
G. Wagner and K. Wüthrich, Observation of internal mobility of proteins by nuclear magnetic resonance in solution, Methods Enzymol. **131**, 307-328, 1986.

[16] J. R. Havens and J. L. Koenig, Applications of high-resolution carbon-13 nuclear magnetic resonance spectroscopy to solid polymers, Appl. Spectrosc. **37**, 226-249, 1983;
F. A. Bovey, New directions in the nuclear magnetic resonance spectroscopy of polymers, Polym. Eng. & Sci. **26**, 1419-1428, 1986.

The initiator-catalyst system [17]

As demonstrated elsewhere, many metal-acetyl acetonates, in combination with very different phenolic compounds, can be used to bring about the polymerization of epoxides, but the most effective one is the combination of $Al(acac)_3$ with catechol (*ortho*-dihydroxybenzene) [18]. When this combination reacts with cyclohexene oxide (as a 'model monomer'; see fig. 3), a polymer is formed as shown in *fig. 13*. As can be seen, catechol acts as the initiator, while $Al(acac)_3$ is the catalyst.

During the polymerization an intermediate can be observed by ^{1}H-NMR spectroscopy. This same intermediate also arises when $Al(acac)_3$ and catechol react with each other *in the absence of epoxides*. Closer study of the reaction product reveals that a dimer structure is formed. This is preceded by a 'ligand' exchange, in which an acetyl-acetone group makes way for a catechol group [17] (*fig. 14*).

Because of this dimerization an intramolecular hydrogen bridge can form between the two phenolic groups present in the dimer, resulting in a strongly 'acidic' proton. As we have seen earlier, an acid can catalyse the polymerization of epoxides.

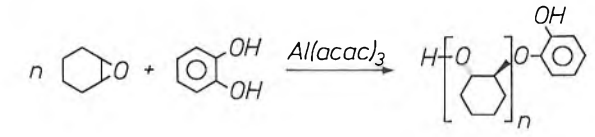

Fig. 13. The polymerization of cyclohexene oxide (fig. 3*e*) using the combination of $Al(acac)_3$ and catechol.

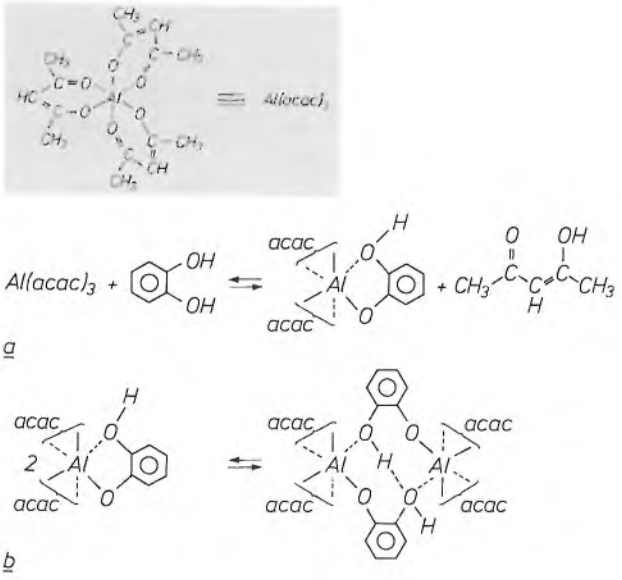

Fig. 14. Reactions for ligand exchange between $Al(acac)_3$ and catechol (*a*) and for dimerization (*b*). See also fig. 15.

The dimer consists of a complex combination of three geometrical isomers. In solution these isomers are in equilibrium with each other, and there is also a monomer-dimer equilibrium (see *fig. 15*). Both equilibria have been investigated in detail by NMR spectroscopy [17].

The mechanism of linear-chain polymerization

As we have seen, dimer formation is essential for effective catalysis and initiation. Two important reaction steps are evidently necessary for polymerization. In the first place the catechol must be activated to open the first epoxide ring; this is done by the ligand exchange with $Al(acac)_3$. In the second step this ligand exchange results in the formation of the dimer; this is the 'acid' dimer that acts as the actual catalyst in the polymerization. Since the re-formed catalyst $Al(acac)_3$ is normally an electrically neutral non-ionic compound, it does indeed seem possible to obtain polymerization in this way without a residue of ionogenic 'contamination'.

By using chromatography and titration we were able to demonstrate that the formation of the dimer is very rapid, in appropriate conditions, and that the propagation step of the polymerization is the rate-determining step (*fig. 16*). It can also be deduced from the figure that the polymerization is just as fast with the combination of $Al(acac)_3$ and catechol as it is with a dimer obtained by separate synthesis. The figure also shows that the polymerization stops when the initiator catechol is used up. This is because the absence of the initiator makes further dimer formation impossible, so that both initiation and propagation of the polymerization come to a stop.

The need for the presence of an acid catalytic dimer suggests that the polymerization takes place via a cationic mechanism (and not for example via a coordinative mechanism, in which an epoxide is repeatedly inserted between the aluminium atom and the growing chain).

In an attempt to obtain further evidence of a cationic mechanism in the epoxide polymerization that we were studying, we investigated a special epoxide monomer, exo-2,3-epoxy-norbornane (structure *a* in *fig. 17*), which served as a model. In a series of experiments we tried to polymerize this compound by using a number of different catalysts. We found that polymerization was not produced by anionic or coordinative catalysis, but only when the catalysis contained a cationic mechanism. The observation that exo-2,3-epoxy-norbornane also polymerizes with a combination of $Al(acac)_3$ and catechol, or with the dimer, is therefore another indication of the cationic nature of this system.

Characterization of the polymer obtained from the acid-catalysed polymerization of exo-2,3-epoxy-norbornane revealed that a Wagner-Meerwein rearrangement takes place during this polymerization. In such a rearrangement the normal 2,3-substitution (structure *b* in fig. 17) does not occur in the polymer produced, but a 2,7 substituted product is obtained instead (structure *c* in fig. 17).

To prove that such an abnormal substitution took place, we subjected the polymer formed to a number of two-dimensional spin-spin decoupling correlated-spectroscopy (COSY) experiments [19] (*fig. 18*), in which we compared the spectrum of the polymer with that of low-molecular compounds like 2,7-dihydroxy-norbornane.

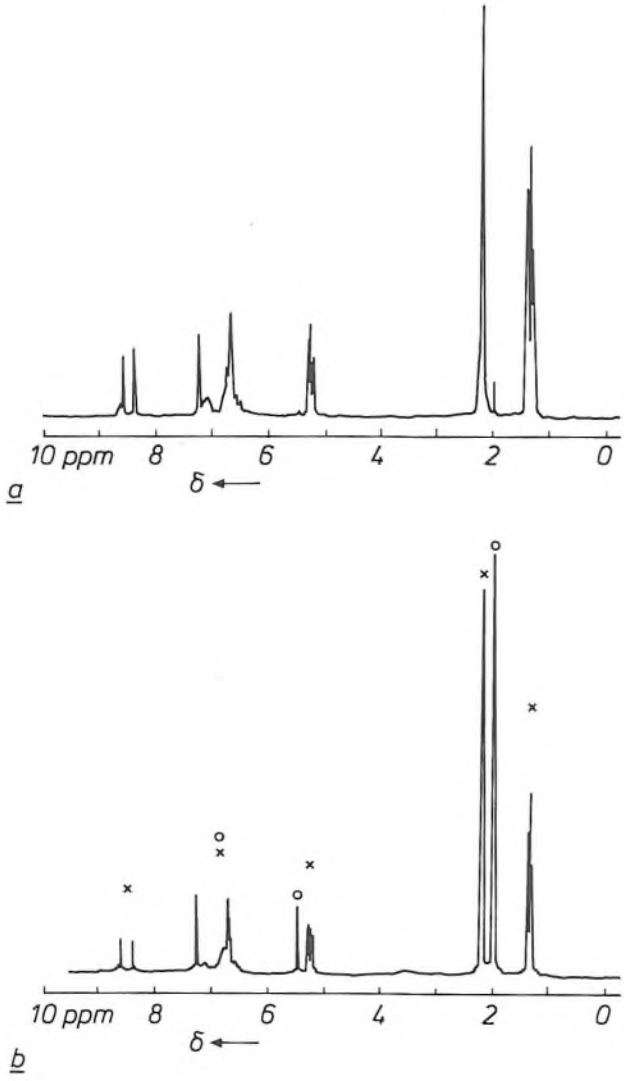

Fig. 15. *a*) ^{1}H-NMR spectrum of a freshly made solution of the dimer in $CDCl_3$. Note the appearance of different resonances for the acetyl-acetonate groups at δ = 1.2 and 5.2 ppm (parts per million) and the three 'acid' protons at δ = 8-9 ppm. *b*) ^{1}H-NMR spectrum of a solution of the dimer in $CDCl_3$ after 2 hours at room temperature. The resonances indicated by an asterisk * correspond to the dimer, and those indicated by o to the monomer.

Polyepoxide network formation

In further investigation of the network formation of bisepoxides initiated and catalysed by the combination of catechol and $Al(acac)_3$, we encountered an

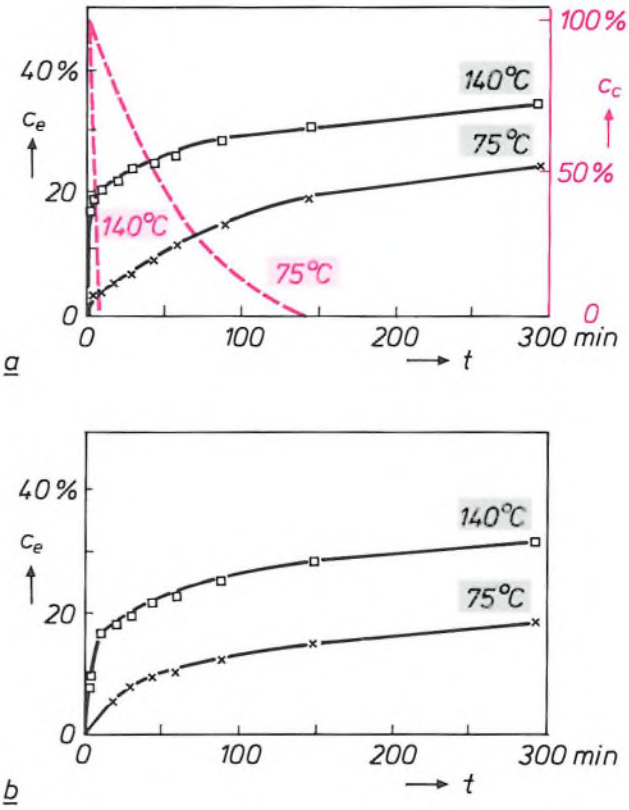

Fig. 16. The percentage c_e of the epoxide conversion for cyclohexene oxide with the combination of $Al(acac)_3$ and catechol (*a*) and with dimer (*b*) plotted as a function of the reaction time *t* of polymerization at T = 140 °C and 75 °C. The concentration of catechol c_c as a function of the reaction time is also shown in 16*a*.

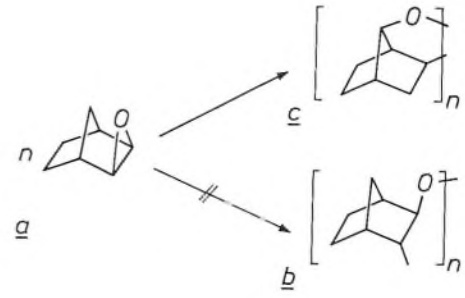

Fig. 17. Structure of exo-2,3-epoxy norbornane (*a*; see also fig. 3*f*), a 2,3-substituted norbornane (*b*) and a 2,7-substituted norbornane (*c*).

[17] E. W. Meijer, The synthesis and structure of bis(acetylacetonato) (2-hydroxyphenolato) aluminium: a stable dimer, Polyhedron **6**, 525-529, 1987.

[18] M. Markovitz, Controllable reactivity epoxy resin hardeners, in: Chemistry and Properties of Crosslinked Polymers, S. S. Labana (ed.), Academic Press, New York 1977, pp. 49-58.

[19] R. Benn and H. Günther, Moderne Pulsfolgen in der hochauflösenden NMR-Spektroskopie, Angew. Chem. **95**, 381-411, 1983.

additional complicating factor: the dimeric initiator-catalyst was not always soluble in the bisepoxides selected. We found, however, that this complication could also be turned to good use.

One of the bisepoxides that we studied was (3,4-epoxycyclohexyl)methyl-3′,4′-epoxyclohexane carboxylate (see fig. 3). We polymerized this compound under various reaction conditions. The reactions were monitored by titration and by determining the gel point.

From this investigation we drew the following conclusions:

- The dimer in the dissolved form is the best initiator-catalyst.
- If the dimer is added in the solid form, the polymerization does not take place or only very slowly at low temperatures, because the dimer dissolves only slightly.
- At higher temperatures fast polymerization and cross-linking do take place with a solid dimer, though

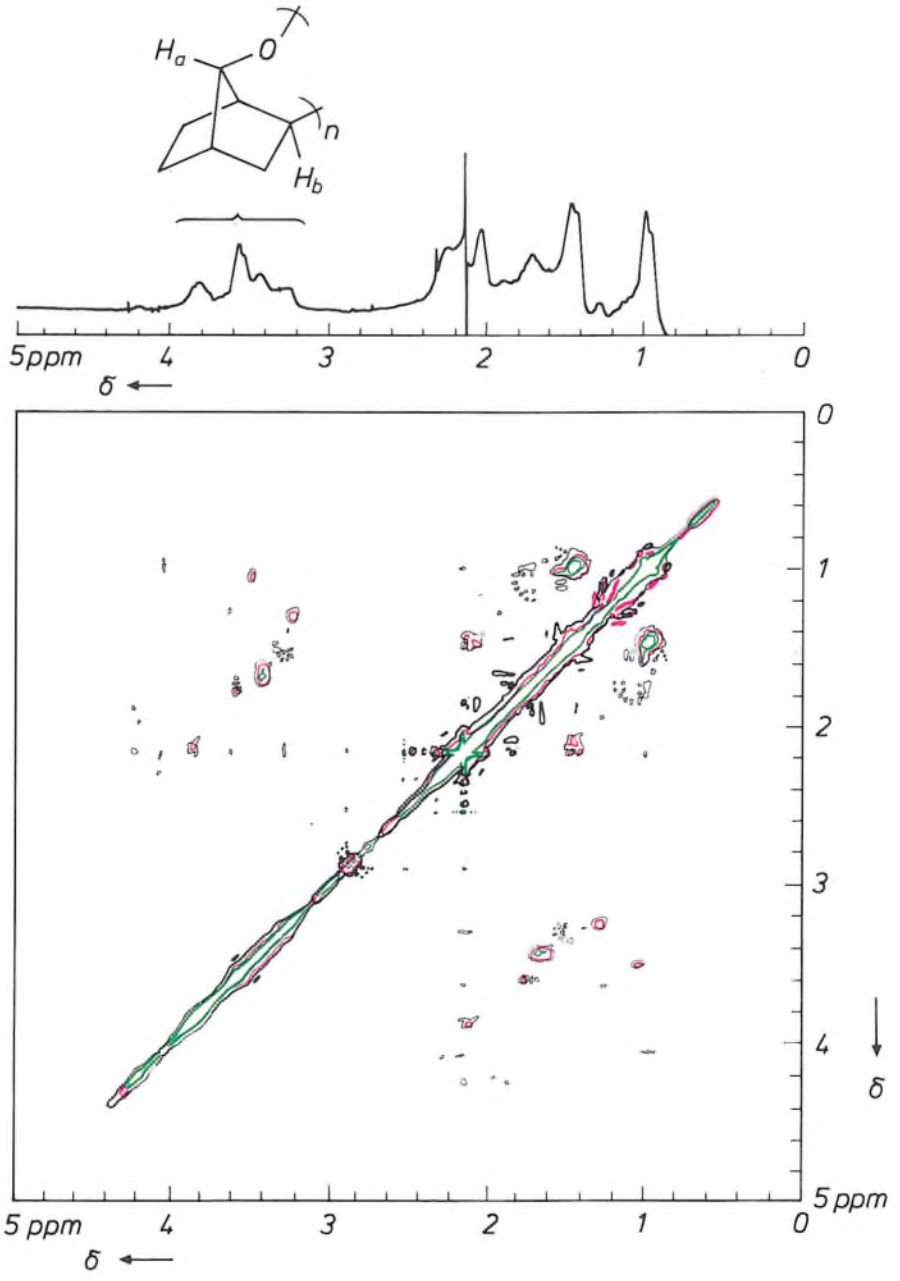

Fig. 18. ^{1}H-NMR and COSY spectra of the polymer of exo-2,3-epoxy-norbornane. COSY experiments (COrrelated SpectroscopY) indicate whether there is a spin-spin coupling between two hydrogen atoms. This coupling appears as a cross peak in the two-dimensional spectrum, where the normal ^{1}H-NMR spectrum appears as a diagonal in the contour picture. The absence of spin-spin coupling between the hydrogen atoms H_a and H_b in the polymer (between $\delta = 3.1$ and 4.0 ppm) is a strong indication that these atoms are in a 2,7 and not in a 2,3 relationship.

only after some delay. Initially, a reaction is only possible at the interface between the solid dimer and the liquid bisepoxide. The dimer is more soluble in polymerized bisepoxide, so that the rate of polymerization increases during the reaction.

- The temperature dependence of the rate of polymerization is not described by a simple Arrhenius equation, because of an irreversible change in the solid dimer [17].
- In the case of the catechol/$Al(acac)_3$ combination we have a situation intermediate between the two cases mentioned above (*fig. 19*).

The above conclusions show that the addition of the dimer in solid form produces a latent initiator-catalyst system.

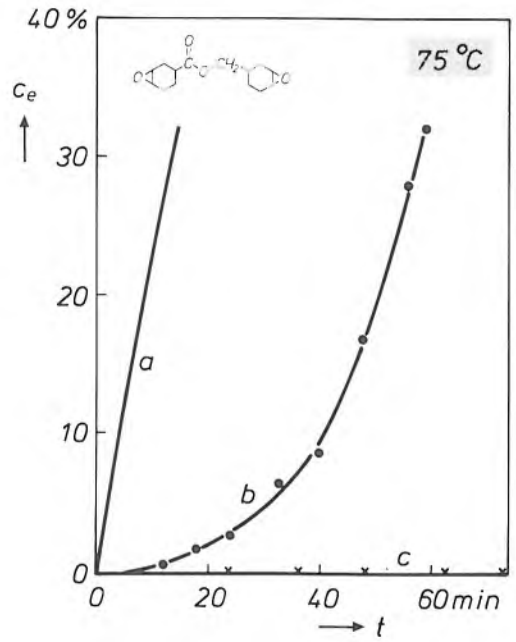

Fig. 19. The epoxide conversion (c_e) as a function of polymerization time t, as measured by means of titration. It is found to make a great difference whether the dimer is added (*a*) in a solution (of $CHCl_3$) or (*c*) as a solid. *b*) Progress of the epoxide conversion with the combination of $Al(acac)_3$ and catechol.

A polymer network that can be built up from such a two-phase situation has the advantage of remaining stable for a long time at low temperatures; fast polymerization and cross-linking can only take place at high temperatures, because a homogeneous reaction mixture is then formed.

Good use can be made of this form of latent catalysis in the production of polymer networks, if at least the perfectly homogeneous phase is reached. If the solid phase is excessively reactive and insufficiently soluble in the reaction mixture, the inevitable result will be an inhomogeneous polymer network. The associated problems are still the subject of investigation.

The two investigations described have been chosen to give some idea of the approach now possible in this sector of chemistry. One shows how phosphorescence spectroscopy can be used to find the relationship between the molecular mobility and the physical properties, and the other how nuclear-magnetic-resonance spectroscopy can help in sorting out the highly complex reaction mechanisms. Both have given a better understanding of the relation between the structure and properties of polyepoxides.

Summary. The polymerization of epoxide monomers with catalysts or initiators results in polyepoxides. Special attention is given to chain polymerization from bisepoxides: the three-dimensional networks formed permit a wide variety of applications. Methods of gaining a fundamental understanding of the formation of these networks and their structure are illustrated by two examples. In the first example it is shown how phosphorescence spectroscopy can be used to monitor changes in the molecular mobility of polymer segments, both during the formation of the network and as a function of temperature. In the second example it is shown how nuclear-magnetic-resonance spectroscopy can be used to study the mechanism of network formation with the aid of model compounds. Emphasis is placed here on the part played by the $Al(acac)_3$/catechol initiator-catalyst system.

1938 THEN AND NOW 1988

Antennas

Antennas are the 'mouths and ears' of many electrical communications systems. They very largely determine the distances over which radio signals can be transmitted and the frequencies that can be used. Their shape and form is of almost limitless variety and depends on the particular application. Half a century ago short-wave radio broadcasting was an important means of communication between the various continents. A special antenna for transmissions on about 10 MHz (a wavelength of about 30 m) was built in the Netherlands. This consisted of two wooden towers, 60 metres high, with a number of vertical half-wave antenna wires attached to them (black-and-white photograph)[*]. The entire structure could be rotated and was mounted on a circular rail system with an outer diameter of just over 46 metres.

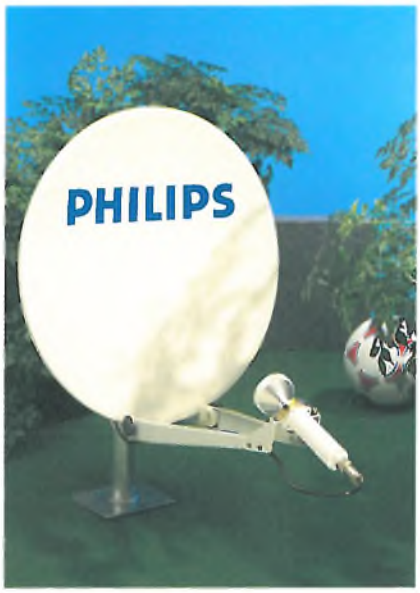

In 1988 we have very many more broadcasting systems. In one of the newest ventures television signals are directly transmitted via a geostationary satellite that stays apparently stationary at a height of about 36 000 km (22 500 miles) above the earth (Direct Broadcasting Satellite). Special antennas give direct individual reception from the satellite. Since the frequencies used are higher than 10 GHz the antennas for transmission and reception are not made from wires, but are parabolic dishes. These act as reflectors for the actual transmitting or receiving element located at the focus. The colour photograph shows a modern version of a satellite receiver antenna with an offset feed. This is designed to bring the focus close to the bottom of the dish, so that the almost vertical antenna is directed towards the satellite. Because of the high quality of the receiving equipment this antenna need only have a diameter of about 55 cm (22 inches). With a satellite, one or more television programmes can be transmitted to an entire continent. It is also possible to take advantage of the full potential of the new and improved television standards such as D2-MAC and HD-MAC[**].

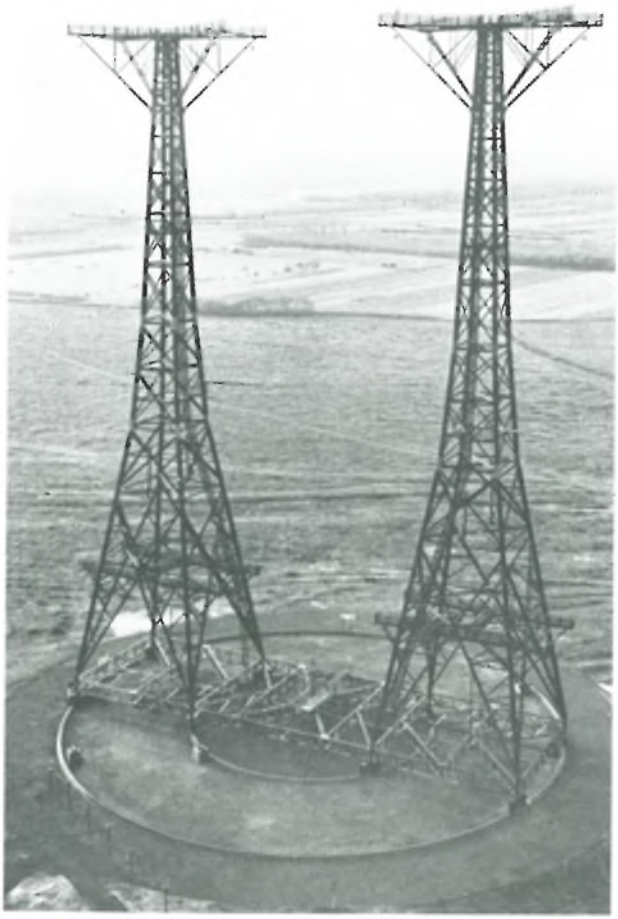

[*] From Philips Technical Review, February 1938.
[**] See for example: M. J. J. C. Annegarn *et al.*, HD-MAC: a step forward in the evolution of television technology, Philips Tech. Rev. **43**, 197-212, 1987.

Theory and practice of acoustic noise control in electrical appliances

J. Crucq

'Life is full of sounds and we want to hear the pleasant and vital ones, while shunning the unpleasant and dangerous variety.' So wrote R. B. Lindsay in his historical introduction to a reissue of Lord Rayleigh's famous standard work 'The Theory of Sound' [*]. *How appropriate that today, with the Compact Disc delighting the ear with agreeable sound, there is renewed interest in the suppression of sound that is less welcome. Noise suppression has become an increasingly important aspect of the design of electrical appliances. It has provided some of the motivation for studies in recent years at Philips Research Laboratories in Eindhoven that are yielding a more fundamental understanding of the generation and suppression of unwanted sound.*

Introduction

In nearly all electrical equipment and appliances — shaver, Compact Disc player, television set or X-ray diagnostic machine — some attention must be given to noise suppression at the design stage. Noise suppression must be based on a fundamental understanding of the physical mechanisms responsible for the origin and transmission of sound [1]. When a good understanding of the fundamentals is available, there is often no need to resort to an empirical approach, which usually amounts to taking a number of steps to reduce noise and measuring the effect of each step separately.

Noise suppression for an appliance still on the drawing board is not usually realistic. What is generally done, therefore, is first to identify the different sources of acoustic noise in a prototype or production model. The next step is to establish the sound power level of the individual sources, usually in dB with respect to a level of 10^{-12} W. The results should then show which sources contribute most to the total noise produced. The investigation should be aimed at these sources first of all. This involves characterizing the sources by the frequencies of the constituent components of the noise signal and by their behaviour as a function of the load and other operating conditions.

The process of transferring the sound from a given source to the environment contains a number of steps: excitation, transmission and acoustic radiation. Excitation is the mechanism that produces vibration. In an electric motor, for example, vibration is due to rotor imbalance or the carbon brushes striking the segments of the commutator. Transmission is the transfer of vibration from the source to other parts of the mechanical structure and therefore also to the outside of the appliance. Acoustic radiation is the conversion of vibration at the exterior of the appliance into airborne sound waves.

The relationship between excitation, transmission and radiation can be shown for each link in the

Ir J. Crucq is with Philips Research Laboratories, Eindhoven.

[*] J. W. Strutt, 3rd Baron Rayleigh, The theory of sound, parts I and II, Dover, New York 1945.

[1] P. M. Morse, Vibration and sound, Am. Inst. of Physics, 1976;
J. P. den Hartog, Mechanical vibrations, McGraw-Hill, New York 1956;
W. C. Hurty and M. F. Rubinstein, Dynamics of structures, Prentice-Hall, Englewood Cliffs, N.J., 1964;
L. L. Beranek, Acoustics, McGraw-Hill, New York 1954.

sound-transfer chain by writing an equation based on an analogy with electrical networks:

$$F = vZ, \tag{1}$$

where F is the force associated with the vibration, v the velocity, and Z the mechanical impedance; all these quantities are complex. F is equivalent to the voltage and v to the current in this 'mechanical Ohm's law'.

If we only consider r.m.s. values of F and v [2], then for the excitation we have:

$$F_{1,\mathrm{rms}} = v_{1,\mathrm{rms}} |Z_1|, \tag{2}$$

where $v_{1,\mathrm{rms}}$ is the r.m.s. value of the velocity of the vibration at the point of action of the alternating force of r.m.s. value $F_{1,\mathrm{rms}}$, and Z_1 is the mechanical input impedance of the structure at this position. The quantities in this and the following equations are thus all position-dependent and are also functions of the frequency f of the vibration. For the propagation of the vibrations through the appliance we have:

$$v_{2,\mathrm{rms}} = H v_{1,\mathrm{rms}}, \tag{3}$$

where H is the real, averaged transfer function of the structure and $v_{2,\mathrm{rms}}$ is the r.m.s. value in time and position of the velocity of the vibration at the cabinet or casing of the appliance. The power P of the sound waves that are 'radiated' from the casing into the surrounding air is then given by:

$$P = \mathrm{Re}(Z_2)\, v_{2,\mathrm{rms}}^2, \tag{4}$$

where Z_2 is the mechanical radiation impedance of the casing.

The mechanical radiation impedance is thus defined as the complex ratio of force to velocity (eq. 1). Another relevant quantity, the acoustic radiation impedance, is defined as the ratio of the pressure to the volume flow of the gas in which the radiated vibration propagates. The mechanical and acoustic radiation impedances are mathematically related through the ratio S^2:1, where S is the area.

Equations (2) to (4) provide an expression for the radiated sound power:

$$P = \mathrm{Re}(Z_2) \left(\frac{F_{1,\mathrm{rms}} H}{|Z_1|} \right)^2, \tag{5}$$

which does not contain the velocities of the vibrations in the structure. From this equation we can draw up a 'recipe' for reducing the noise output from an electrical appliance:

- reduce the excitation force F_1,
- increase the mechanical input impedance Z_1 of the structure,
- prevent the propagation of the vibration by decreasing the transfer function H, and
- reduce the acoustic radiation by decreasing the real part of the mechanical radiation impedance Z_2.

The first three items produce the most effect, since the associated factors occur as the square in equation (5).

At Philips Research Laboratories acoustic investigations have been carried out on various Philips products, including vacuum cleaners, food processors, fluorescent lighting switchgear, Compact Disc players and television deflection coils. The theoretical considerations outlined above will be illustrated by a description of our investigation of the noise generated by a washing machine and a refrigerator.

The washing machine whose noise output was investigated was a front-loader, i.e. one in which the wash is contained in a drum accessible from the front. The drum rotates in a 'tub', which can be partly filled with water or suds; see *fig. 1*. In a complete wash programme the machine works through the three main modes of operation: wash, at a drum speed of 50 revolutions per minute; rinse, at the same speed; spin drying, at a maximum speed of 850 revolutions per

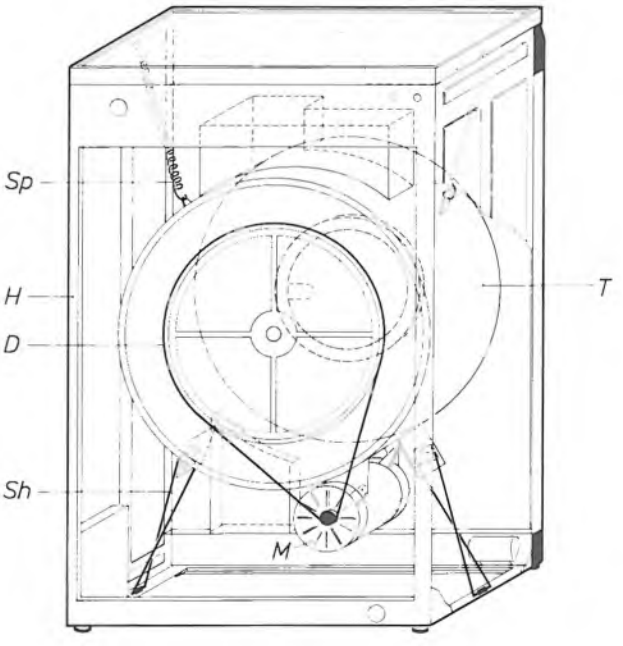

Fig. 1. The interior of a front-loading Philips washing machine. *Sp* spring. *H* cabinet. *D* V-belt drive. *Sh* shock-absorber. *M* motor. *T* tub, filled with water or suds. The drum (not shown) rotates in the tub. The view is from the back of the machine. The wash is put into the tub from the other side of the machine.

minute. (In the latest Philips washing machines this speed can be even higher.)

In a washing machine several sources of noise can be identified, such as:

- the motor,
- the V-belt drive and the ball-bearings of the drum,
- the wash moving in the liquid, and
- the pump for draining the suds or rinsing water.

This article will be mainly concerned with the motor and its power supply. We shall see that the thyristor speed-control system is a major source of noise. Power-supply modifications and some changes in design have made the latest Philips washing machines, such as the AWB 991, very much quieter, see *fig. 2*.

The main source of noise in a refrigerator is the compressor unit; see *fig. 3*. The compressor increases the pressure of the gaseous refrigerant, a fluorocarbon called Freon, from 1.2 bars to about 14 bars. The compressed gas is liquefied in a condenser outside the actual refrigerating compartment. The pressure of the liquid refrigerant decreases in a capillary restrictor, and the liquid is then returned to the gaseous form in the evaporator against the rear wall of the refrigerating compartment. This is the process for extracting heat from the refrigerating compartment.

In our investigation we treated the compressor unit as an independent device, containing various separate noise sources. The most important ones are:

- the intermittent induction intake of the gas,
- the alternating forces on the piston due to compression of the gas, and
- the intermittent discharge of the gas under pressure.

In this article we shall only consider the intake of the gas, one of the main sources of noise in refrigerator compressors until recently. It will be shown that the noise from this source has been considerably reduced in intensity by modifying the intake silencer (silencers are sometimes called 'mufflers'). The proposed modification has given a reduction of 3 dB(A) [3] in the noise level from the compressor unit built into many Philips refrigerators, such as the ARG 197 refrigerator-freezer; see *fig. 4*.

The intake silencer was improved by optimizing its operation as a reactive silencer. A silencer of this kind usually consists of a number of expansion chambers as in fig. 3, linked by tubes. The noise is attenuated in the silencer because the acoustic input impedance of the silencer is mainly reactive and not matched to the internal impedance of the source. Because of this mismatch, the sound source delivers less power than without the reactive silencer. The action of the reactive si-

Fig. 2. The Philips AWB 991 washing machine. In this machine the speed of the drum is 1200 revolutions per minute during spin-drying.

Fig. 3. The interior of an earlier version of one of the Philips compressor units for refrigerators. The two circular expansion chambers of the intake silencer can be seen at the top right. Units of this type, in an improved version, are produced in large numbers by the Philips factories in Cassinetta, Italy.

[2] The 'r.m.s. value' is understood here to be the root-mean-square value in a narrow frequency band. Defined in this way the r.m.s. value is in general frequency-dependent.

[3] The 'A' in dB(A) indicates that a weighting is applied at each frequency from a standardized curve, the A-weighting curve, which correlates with the sensitivity of the human ear.

Fig. 4. The Philips ARG 197 refrigerator-freezer. The refrigerator is at the top, the freezer below. The appliance has only one compressor unit and has electronic temperature control, with a temperature sensor in both the refrigerator and freezer compartments. The control circuit operates a valve that divides the refrigerant between the two evaporators in the two compartments.

lencer can also be considered as the result of destructive interference of incident and reflected sound waves. The waves are reflected from one of the successive discontinuities in the silencer. The principle of the reactive silencer has also been used to suppress the exhaust noise from Philips vacuum cleaners [4].

The analysis of the vibration in the washing machine will be considered first, and then the measures taken to reduce the vibration. The same procedure will be followed for the refrigerator compressor.

The washing machine

General

Before making any acoustic measurements or calculations it is first advisable to listen carefully. When we listen to a washing machine a number of clearly identifiable sounds can be heard. These originate from sources such as the pumps and the wash and spin-drying operations. Any assessment of these sounds has to include a rather subjective view of the amount of annoyance and their duration. It turns out that washing makes less noise than spin-drying, but that the noise is more annoying and lasts longer. The noise from the pumping is also annoying, but does not last very long. This can be reduced fairly easily by mounting the pump on vibration isolators.

In view of the foregoing the discussion here will be limited to our investigation of the noise produced during the wash operation. In the washing machine we investigated the drum is driven by a d.c. motor that has a speed of 800 rev/min during the wash cycle. The drum speed is then 50 rev/min. The stator field in the motor is produced by two permanent magnets. The motor was designed for use in washing machines [5]; the torque and hence the speed of the motor can easily be varied by changing the mean value of the current in the rotor windings. The same motor can therefore be used for wash and spin dry.

The mean current in the rotor windings is varied by means of an electronic circuit containing thyristors. This circuit rectifies the alternating current from the mains and prevents the flow of current during a preset part of the period of 10 ms; see *fig. 5a*. The motor speed is measured by means of the e.m.f. induced in the rotor windings. A control circuit compares the actual speed with the desired value. Any difference results in a change of the time at which the thyristors are triggered. The circuit thus gives a sudden increase in the rotor current once every 10 ms.

These periodically repeated sharp increases in the rotor current and the corresponding discontinuities in the motor torque could be a major cause of the noise produced during the wash cycle. To verify this hypothesis we measured the noise spectrum during the wash operation under two conditions: one with the normal supply from the mains via thyristors, and the other with the motor receiving its power from a stabilized direct-current source.

The measurements were performed in the special non-rectangular reverberation chamber at Philips Research Laboratories in Eindhoven [6]. The large number of reflections from non-parallel walls in this chamber give a virtually diffuse sound field, with a simple relation between the sound pressure and the power radiated by a source. The r.m.s. sound pressure at various frequencies was measured with 'one-third octave band filters'. The measurements were converted into sound power and plotted in dB. In addition to each spectrum, the noise power summed over all the frequency bands measured was also plotted in dB(A).

The noise spectra measured in this way are shown in fig. 5*b* and *c*. Comparison shows that the noise reduction due to stabilizing the power supply is very considerable: the total noise power has fallen by 13 dB(A). The most important source of noise during

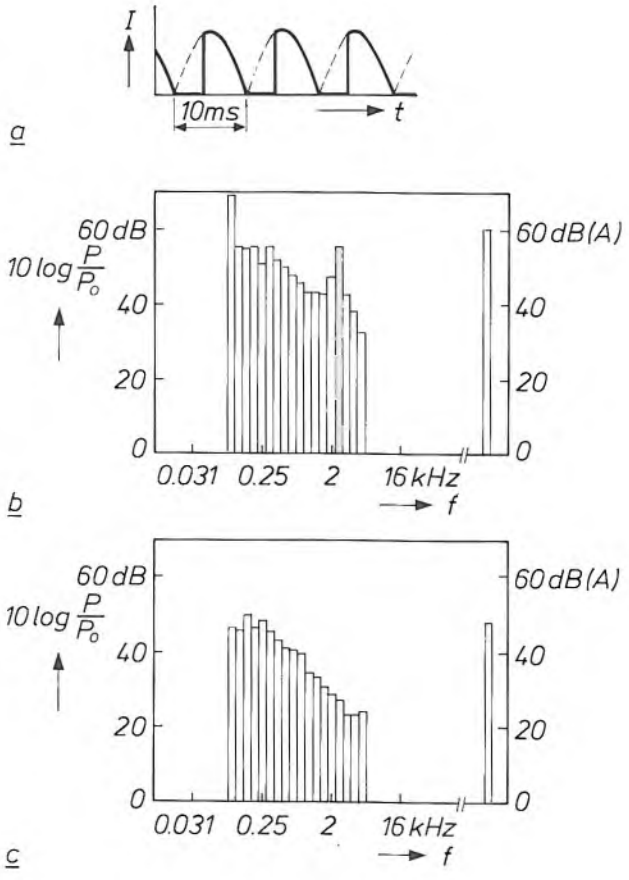

Fig. 5. *a*) The motor current I as a function of time t. During a part of a period of 10 ms (half the period of the alternating current from the mains) the flow of current is prevented by a thyristor; it then increases suddenly. *b*) Noise spectrum of the washing machine in fig. 1, measured during the wash cycle. The spectrum shows the ratio in dB of the noise power level P to a reference level P_0 of 10^{-12} W as a function of frequency f. Each bar indicates the noise power measured within a band of 1/3 octave. The shaded bar relates to the 1/3 octave band at 2.5 kHz. The bar on the far right relates to the ratio to P_0 in dB(A)[3] of the noise power summed over all frequencies. *c*) A noise spectrum measured in the same way but with a stabilized direct voltage for the motor.

the wash cycle has thus been identified: vibration in the motor due to the sudden rise in the motor current every 10 ms.

Analysis of the motor vibration

After the main source of the noise produced during the wash cycle has been identified, it is necessary to gain a better understanding of the mechanism of the vibration in this source. Only then will it be possible to take the appropriate measures to reduce this vibration. We started by measuring the noise spectrum of the motor alone, running at the speed used during the wash cycle.

Fig. 6a shows a cross-section of the motor. The measured noise spectrum is shown in fig. 6*b*. If we compare the spectrum with that of the washing machine in operation (fig. 5*b*), we see that both spectra have a peak (shaded) in the 1/3-octave band at 2.5 kHz.

Our next step was to attach two accelerometers to the housing *Ho* of the motor, as indicated in fig. 6*c*. We struck the housing with a hammer and recorded the two damped oscillations; see fig. 6*d*. The resonant frequency of the stator is the same for both signals: 2600 Hz. This value corresponds to the peak in the noise spectrum in the 2.5-kHz 1/3-octave band. The measured acceleration amplitudes and phase difference suggest that the permanent magnets oscillate in opposition in this resonance. The tubular housing then acts as a relatively weak spring linking the magnets.

Further comparison of figs 5*b* and 6*b* shows that the noise power in the 1/3-octave band at 2.5 kHz is 3 dB higher in the spectrum of the washing machine. In the transmission of the motor vibration to the tub and the cabinet something seems to be added to the power. However, the cabinet is in fact intended to provide sound insulation for the sound radiated from the motor. In other frequency bands, especially in the low range, we find even higher contributions to the sound power. It is interesting to consider the part played by the tub, to which the motor is directly attached. Since the tub is fairly large — diameter 50 cm and width 30 cm — it is a good radiator of low-frequency sound.

Analysis of the tub vibration

During the wash cycle we measured the acceleration of the tub, with the accelerometer mounted on its rim; see *fig. 7a*. We see that the vibration spectrum consists mainly of harmonics of 100 Hz. These harmonics are excited by the pulses in the motor current. For a closer analysis we mounted a second accelerometer on the other side of the tub. During the wash we recorded the two signals simultaneously and analysed them with a two-channel FFT analyser (FFT: Fast Fourier Transform). This analyser can measure both the amplitudes and the phase difference of two signals in a particular frequency range.

The FFT analysis shows that in the range below 600 Hz the 100-Hz harmonics of both signals are equal in amplitude but opposite in phase. This suggests that the vibration of the tub is a 'rigid-body oscillation'; see fig. 7*b*. At low frequencies the tub assembly with its sprung suspension can therefore easily be approximated by a mass-spring system. Significant resonances from the walls of the tub only appear in the range from 600 to 900 Hz. Fig. 7*c* shows for

[4] Plastics in vacuum cleaners, Philips Tech. Rev. 44, 43, 1988.
[5] R. Raes and J. Schellekens, A speed-controlled d.c. motor for a washing machine, Philips Tech. Rev. 34, 163-169, 1974.
[6] J. M. van Nieuwland, A. Petterson and C. Weber, The design and construction of a non-rectangular reverberation chamber, Philips Tech. Rev. 37, 176-179, 1977.

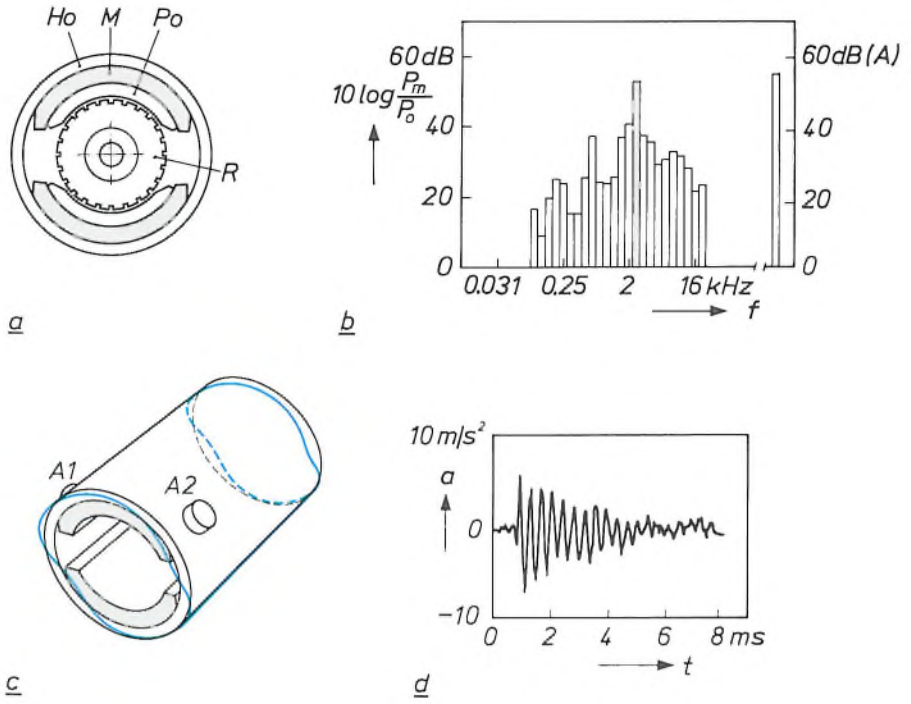

Fig. 6. *a*) The washing-machine motor. *Ho* housing. *M* permanent magnets. *Po* pole pieces. *Ho*, *M* and *Po* form the stator. *R* rotor. *b*) The noise power P_m of the separate motor in dB as a function of frequency f ($P_0 = 10^{-12}$ W). The shaded bar relates to the 1/3-octave band at 2.5 kHz. *c*) The blue lines represent schematically the relative movements of the stator halves during a resonance at a frequency of 2.6 kHz. *A1* and *A2* accelerometers. *d*) The acceleration *a* measured by one of the transducers as a function of time *t*.

example the pattern of flexural vibrations at 630 Hz at the circumference of the tub. The asymmetry of the pattern is due to an irregular distribution of the mass and stiffness of the material at the circumference.

Reducing the vibration

One of the most obvious measures here is to modify the steep leading edges in the motor current. We proposed a modification of the power supply to give a double step in each leading edge, as in *fig. 8a*, with the time between the two steps equal to half a period of the stator oscillations as in fig. 6*c*. The result of the double step is that two oscillations with a phase difference of 180° are excited every 10 ms, as shown in fig. 8*b*. With this phase difference these two oscillations should in theory cancel each other.

In practice the two oscillations do indeed largely cancel out, as figs 8*c* and *d* show. These figures give the results of stator-acceleration measurements for a supply with no steps in the current pulse and with a stepped pulse. The maximum acceleration is much smaller with the modified current pulse.

In the latest Philips washing machines a slightly different solution has been adopted for the problem of the motor power supply. The thyristor speed control has been replaced by a chopper circuit, in which the sinusoidal mains voltage is rectified and then converted by power transistors into pulses at a repetition

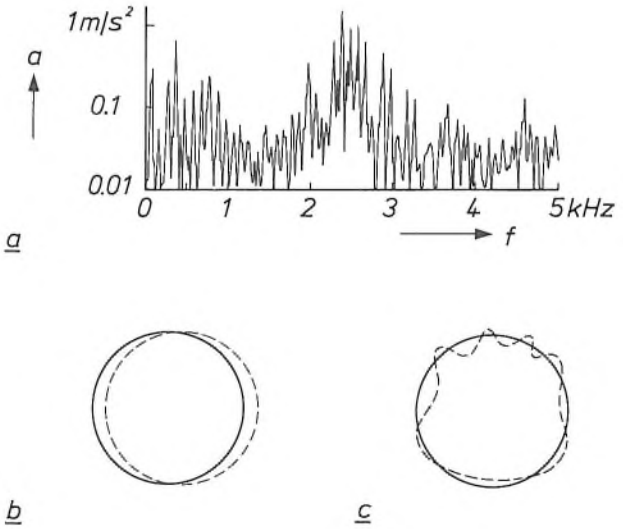

Fig. 7. *a*) The measured r.m.s. value *a* of the acceleration of the tub (*T* in fig. 1) as a function of frequency *f*. *b*) Schematic indication of the movement of the tub during 'rigid body' oscillations. *c*) The pattern for flexural vibrations at 630 Hz at the circumference of the tub.

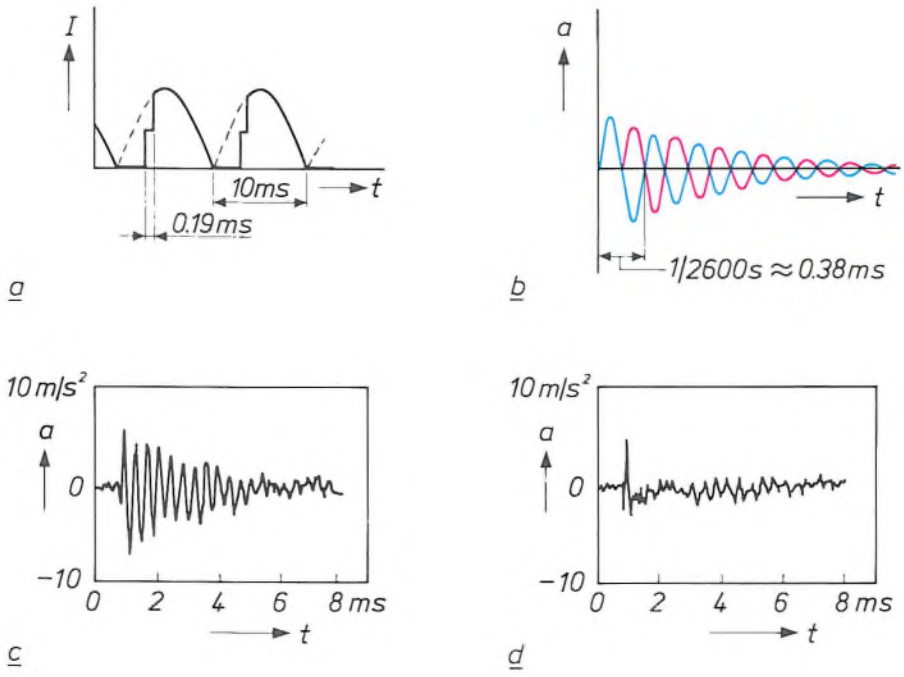

Fig. 8. *a*) The motor current *I* as a function of time *t* with a modified power supply for the motor. A double step appears in the leading edge every 10 ms. *b*) The damped oscillations of the stator halves, as would be expected; see fig. 6*c*. *a* acceleration. *t* time. The oscillations shown in red and blue have a phase difference of 180° and are excited by the first and second steps in *I*. The time of 0.19 ms between the two steps is made approximately equal to half a period of the oscillations at a frequency of 2600 Hz. *c*) The measured oscillations of the stator with the unmodified power supply for the motor, and *d*) with the modified power supply.

rate of about 10 kHz. The width of the pulses is variable. Because of the filtering action of the inductive motor windings the current is virtually a direct current. The mean value of the current and hence the speed of the motor are controlled by varying the width of the 10-kHz pulses. In this circuit the current therefore changes much less abruptly than it did with the thyristor-controlled supply.

Another approach was to improve the motor mounting. Simple rubber rings were replaced by more effective vibration isolators. This and the power-supply modification described above had the effect of substantially suppressing both the actual motor vibration — 100-Hz harmonics and 2600-Hz resonance — and its propagation.

We also improved the sound insulation of the cabinet. In the transmission of the sound from the interior of the machine to the outside world via the casing, three transmission paths are important:

- transmission via the layer of air between tub and cabinet,
- transmission via the springs and shock-absorbers that carry the tub, and
- airborne transmission via holes in the sheet steel of the cabinet.

In the first path the air layer between the tub and the cabinet acts as a relatively stiff spring for the low-frequency 'rigid-body oscillations' of the tub. This spring transmits the low-frequency oscillations of the tub to the sheet-steel sides of the cabinet with very little change in amplitude and vibration pattern. These sheet-steel 'plates' therefore go into a forced flexural vibration, so that large parts of the 'plates' oscillate in phase. The mechanical radiation impedance for flexural vibrations of this kind is high, so that the sound insulation of the cabinet in this situation is almost zero. As we have seen above, the magnitude of the low-frequency oscillations has fortunately been considerably reduced by the measures proposed.

In sound transmission by the second path the sides of the cabinet are excited at the places where the springs and shock-absorbers are fixed. These local excitations set up free flexural vibrations, which differ from the forced type in that different parts of a 'plate' oscillate in antiphase. The wavelength of free flexural low-frequency vibrations is much smaller than that of the airborne sound, so that pressure differences close to the 'plate' are equalized. The acoustic radiation impedance for these free flexural vibrations is thus low. The low-frequency oscillations of the tub shown in

fig. 7*b* and *c* will therefore be almost unable to reach the ambient air by this path.

If the wavelength of the free flexural vibrations in the 'plate' is smaller than that of the radiated sound, the sound waves near the plate will be 'acoustically short-circuited'. The air layers furthest removed from the vibrating plate are then no longer disturbed: the air vibrations die out. The wavelength of sound is inversely proportional to the frequency; the wavelength of free flexural vibrations is inversely proportional to the root of the frequency. The acoustic-short-circuiting effect thus decreases with rising frequency, and vanishes when the wavelength of the air vibrations becomes equal to the wavelength of the free flexural vibrations. The corresponding frequency is called the 'critical frequency' [7]. It is 15 kHz for 1-mm sheet steel, the material generally used for washing-machine cabinets.

In the third path the sound is transmitted to the ambient air through openings in the cabinet. It therefore makes sense to 'plug the leaks' in the cabinet as far as possible. A significant leak is the gap between the cabinet and the floor. Closing this gap is therefore an important noise-reduction expedient. A proposal has also been made to fit absorbent material to dissipate acoustic energy inside the cabinet.

The last, but by no means the least-significant, measure we have proposed relates to a modification of the motor end-shields. These are mounted at the ends of the stator and support the rotor bearings. Openings in the end-shields admit the air for cooling the rotor windings. It has been found that the rotor does not in fact become too hot if these openings are closed. The noise output from the motor is then much lower, however. The effect of running with these openings closed is particularly valuable in the spin-dry cycle, when the motor speed is higher.

Applying the measures mentioned reduces the noise output during the wash by about 5 dB(A).

The refrigerator compressor

General

Fig. 9 shows a cross-section of the compressor unit, which consists of the compressor proper, an electric motor and a hermetically sealed housing of 2.5-mm steel. This housing is called the 'shell'. The reciprocating motion of the piston in the compressor is obtained from crank gear. At every revolution of the crankshaft the intake and outlet valves are opened alternately by the reduced pressure and the excess pressure of the gas in the cylinder.

The motor shaft is hollow, and its lower end dips into a quantity of oil in the bottom of the shell. The hole in the shaft widens, so that oil is drawn into the shaft by centrifugal force. The oil is forced into the crankshaft and from there through the hollow connecting rod to the gudgeon pin. The oil thus lubricates the crankshaft bearings, the two connecting-rod bearings and the piston in the cylinder. Oil is also sprayed from the crankshaft around the cylinder to cool it.

The compressor is spring-mounted in the shell. The Freon gas enters the free space between the shell and the compressor through an inlet channel. The gas is drawn into the cylinder from this space through an intake silencer with two expansion chambers in cascade; see fig. 3. The compressed gas leaves the compressor unit through an output silencer and a metal tube, the discharge tube. This is made as flexible as possible and passes through a gas-tight seal in the wall of the shell.

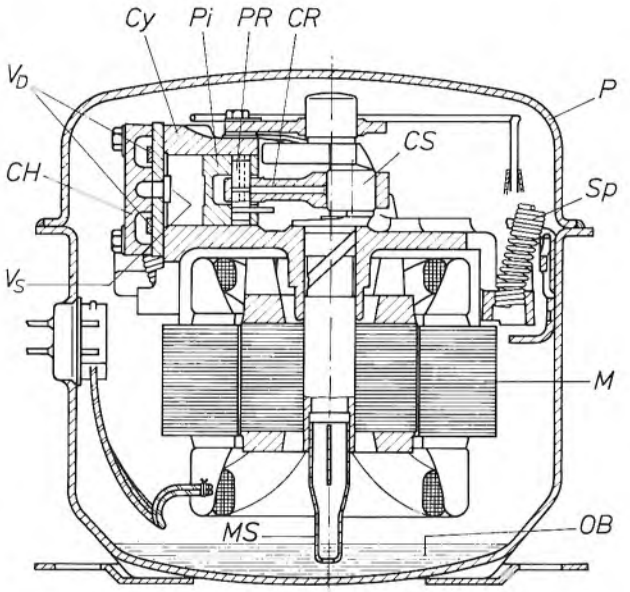

Fig. 9. The compressor unit. V_S inlet valve. *CH* cylinder head. V_D outlet valve. *Cy* cylinder. *Pi* piston. *PR* gudgeon pin. *CR* connecting rod. *CS* crankshaft. *P* shell. *Sp* spring. *M* motor. *OB* oil bath. *MS* hollow motor shaft with 'oil pump': the opening widens towards the top.

The noise sources in the compressor unit, which were mentioned in the introduction, can transfer sound to the wall of the shell via

- the Freon gas,
- the oil reservoir,
- the discharge tube, and
- the three springs of the suspension system.

Finally, the shell wall radiates the sound to the surrounding air.

In our investigation we examined the various possible sources of noise. This entailed first measuring the noise produced both with the source and without the source, if possible. This often meant that modifications had to be introduced. For example, we were able to study the effect of parts of the crank gear by operating the compressor with a lighter piston and with a stiffer connecting rod.

We compared the results of the measurements with the results of calculations based on models. When the results of the calculations were in reasonable agreement with the measurements, the models helped us to find ways of reducing the noise levels.

The investigation of the various sources of noise led eventually to seven proposed modifications to reduce the noise levels. These gave a total reduction of 10 dB(A), without any need to change the functional specifications of the compressor. The design of the model for the noise due to the gas intake will now be considered, as well as the measurements made in investigating this noise.

The model for the intake noise

The intermittent volume flow resulting from the opening and closing of the inlet valve must be considered as the actual source of the intake noise. This flow causes pressure fluctuations that propagate in the intake silencer in the direction of the intake opening. The pressure fluctuations excite acoustic resonances in the gas-filled space in the shell.

This hypothesis can be verified by analysing the oscillations of the wall of the shell after a 'cold start'; this is done by recording a number of frequency spectra in succession. The temperature of the gas in the compressor unit rises from 20 to 90 °C after the cold start. The velocity of sound in the gas in the shell then changes such that:

$$\frac{c_1}{c_2} = \frac{\sqrt{T_1}}{\sqrt{T_2}}, \qquad (6)$$

where c_1 and c_2 are the sound velocities in the gas at the absolute temperatures T_1 and T_2. The wavelength $\lambda = c/f$ of a particular resonance in the gas depends only on the geometry of the space. The resonant frequency f therefore changes with temperature in the same way as the sound velocity. Since the principal resonance peaks in the measured spectra shift to a higher frequency when the gas temperature increases, these peaks are the result of acoustic resonances in the gas. These resonances in turn set the wall in motion. They are not therefore resonances of the wall itself.

For the model that describes the origin, transfer and radiation of the intake noise, we can write the equation:

$$P_{rad} = \frac{P_s}{IL_d \cdot IL_b}, \qquad (7)$$

where P_{rad} is the power of the sound radiated by the shell wall, IL_d is the insertion loss for the sound transmission in the intake silencer and IL_b is the insertion loss for the sound transmission via the gas-filled space and the shell wall. P_s is the power of the sound originating at the inlet valve for the case in which the sound can be directly radiated to the environment, i.e. without silencer and shell. All the quantities in eq. (7) (and those in the next equation) are a function of the frequency f.

For P_s we can write the equation:

$$P_s = Q_{rms}^2 \, \mathrm{Re}(Z_s), \qquad (8)$$

where Q_{rms} is the r.m.s. value of the intermittent volume flow at the inlet valve [2] and Z_s is the acoustic radiation impedance for the sound source formed by the intermittent volume flow in the opening of the inlet valve (without the silencer and shell).

This sound source can be considered as being replaced by a rigid flat piston of radius r, which moves to and fro inside an infinite stationary wall (baffle). In an electrical analogue Z_s can then be approximated by the impedance of a network containing two resistances, a capacitance and an inductance [8]; see *fig. 10*. The inductance in this network is equivalent to the mass of the gas, the capacitance to its elasticity. The resistances show that energy is in fact transferred to the gas. R_1, R_2, C and L can be expressed in terms of ϱ, the density of the gas, c and r.

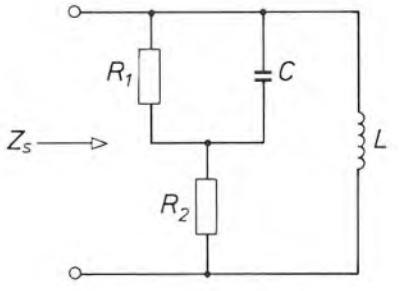

Fig. 10. Electrical analogue for a reciprocating piston in an infinite baffle. The impedance Z_s of the network is analogous to the acoustic radiation impedance of the sound source formed by the moving piston. R_1 and R_2 resistances. C capacitance. L inductance.

[7] See pages 290 to 294 of: L. L. Beranek, Noise reduction, McGraw-Hill, New York 1960.

[8] See pp. 118 ff. of the book by Beranek, note [1].

The sound power at the inlet valve can be calculated as a function of frequency (eq. 8) if the variation of the volume flow as a function of time is known. We used two methods for determining this function $q(t)$. The first is based on the assumptions that the lift of the inlet valve is an exponential function with time constant τ, that the pressure difference Δp across the valve decreases linearly with time after it has been

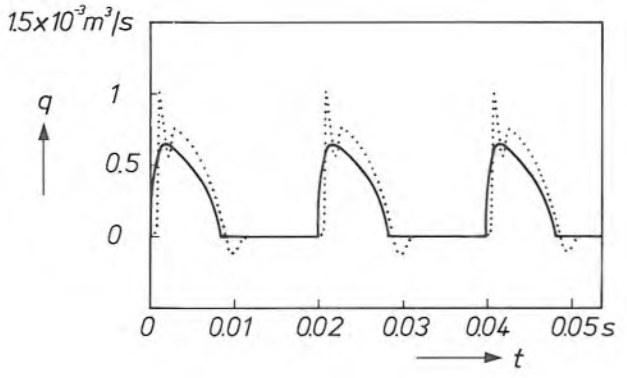

Fig. 11. Two different results of calculations of the volume flow q at the inlet valve of the compressor as a function of time t. The continuous line relates to the result of the calculation from eq. (9), which is based on a number of simplifications in the behaviour of the valve and the gas. The dotted line relates to the result of a computer simulation.

opened, and that the volume flow is proportional to $\sqrt{|\Delta p|}$. From these assumptions it follows that:

$$q(t) = \frac{A}{\varrho}\left(1 - e^{-\frac{t}{\tau}}\right)\sqrt{t_0 - t} \quad \text{for } 0 \leqslant t \leqslant t_0, \qquad (9)$$

where A is a constant that depends on the capacity of the compressor (2.9 kg per hour) and t_0 is the time the inlet valve is open. The quantities τ and t_0 can be estimated from measurements of the height of the valve as a function of time.

In the other method of determining $q(t)$ a computer program simulates the thermodynamic behaviour of the compressor [9]. *Fig. 11* shows the results of both methods of calculation. The computer simulation probably gives a more realistic picture, since it takes the dynamic properties of the inlet valve into account. These can cause fluctuations in the gas flow, which may even become negative.

The insertion loss IL_d of the intake silencer is equal to the ratio of the intake noise power without the silencer to the intake noise power with it. IL_d can be calculated by setting up a transfer matrix H_i for each element of the silencer, which can be an expansion chamber or a connecting tube. This matrix gives the relation between the sound pressure and the volume flow p_i and q_i before the element and p_{i+1} and q_{i+1} after the element:

$$\begin{pmatrix} p_{i+1} \\ q_{i+1} \end{pmatrix} = H_i \begin{pmatrix} p_i \\ q_i \end{pmatrix}. \qquad (10)$$

The transfer matrices for the various elements of the silencer can be calculated with the one-dimensional acoustic wave equation. The transfer matrix H of the complete silencer is given by the product of the matrices of n separate elements:

$$H = \prod_{i=1}^{n} H_i.$$

The insertion loss IL_d can be calculated from the total transfer matrix H and the acoustic radiation impedance. A computer program was written for these calculations, but this will not be discussed here. It can be

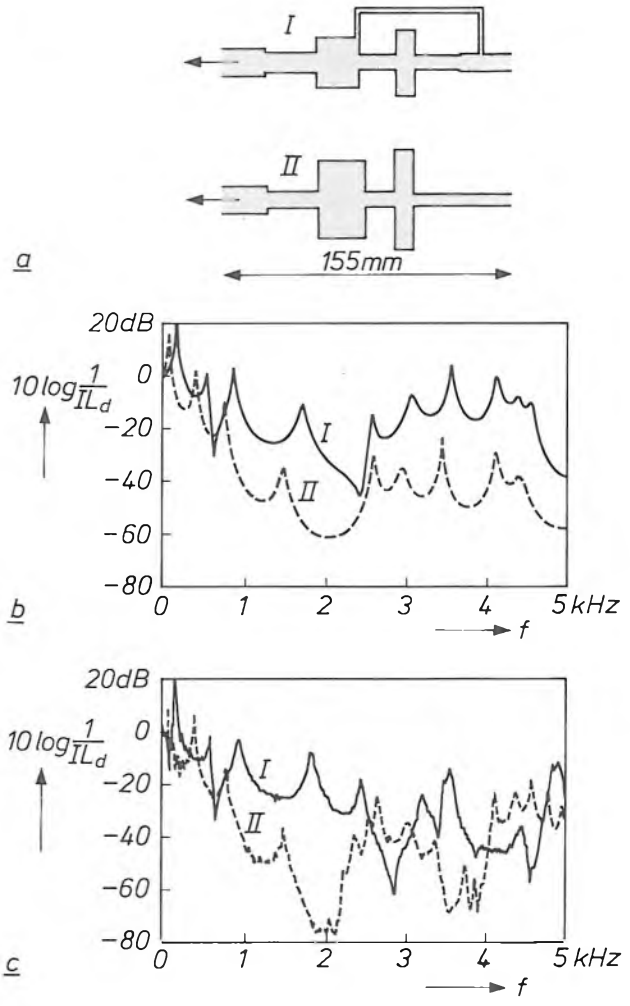

Fig. 12. The results of calculations and measurements for two different intake silencers. *a*) Schematic representation of an earlier version (*I*) and a recent version (*II*) of the silencer. *b*) the reciprocal of the calculated insertion loss IL_d, and *c*) the reciprocal of the measured insertion loss IL_d, both in dB as a function of frequency f for silencers *I* and *II*.

used for comparing the insertion losses of different versions of the intake silencer.

To calculate the insertion loss IL_b for the shell and the free gas volume models would have to be set up for the acoustic resonance of the gas volume, the mechanical resonances in the steel wall of the shell, the coupling between the two kinds of resonance, and the sound radiation from the shell. This could be done by using the finite-element method. However, in this case such calculations would be complex and time-consuming, so we decided to do without and just make a number of measurements.

The calculations and measurements

Fig. 12 shows the results of calculations and measurements of the insertion loss IL_d of two intake silencers. Silencer *I* is an earlier version (see fig. 3) and silencer *II* is the most recent one, introduced largely because of the investigations described in this article. The results of the calculations given in fig. 12*b* are in good agreement with the results of the measurements given in fig. 12*c*. Silencer *II*, which has larger expansion chambers and no parallel tube, has a better insertion loss at nearly all frequencies. At very low frequencies, incidentally, this quantity is found to be smaller than 1, so that the sound is amplified. Other measurements showed that the performance of silencer *I* is even worse if the parallel tube is omitted.

The most obvious method of measuring the insertion loss IL_b for the shell and the free gas volume is to place a small sound source at the mouth of the intake silencer, and then to measure the sound with and without the shell. The problem here is that it is difficult to find a small source that will produce enough sound to give a sufficiently large signal-to-noise ratio outside the shell. We therefore made use of the reciprocity principle, which in this case states that the insertion loss can also be measured by interchanging the source and the measuring device. For our measurements in the reverberation chamber we used two large loudspeaker units and measured the sound at the mouth of the intake silencer with a small microphone. The insertion loss IL_b as a function of frequency is the ratio of the power spectrum measured without the shell to the spectrum measured with it (including the Freon gas).

Conclusion

The previous section showed in general terms how the power of the sound produced by the intermittent volume flow at the inlet valve could be calculated. The calculation of the insertion loss of the intake silencer has also been treated. The insertion loss for the shell and the free gas volume was measured in the way just

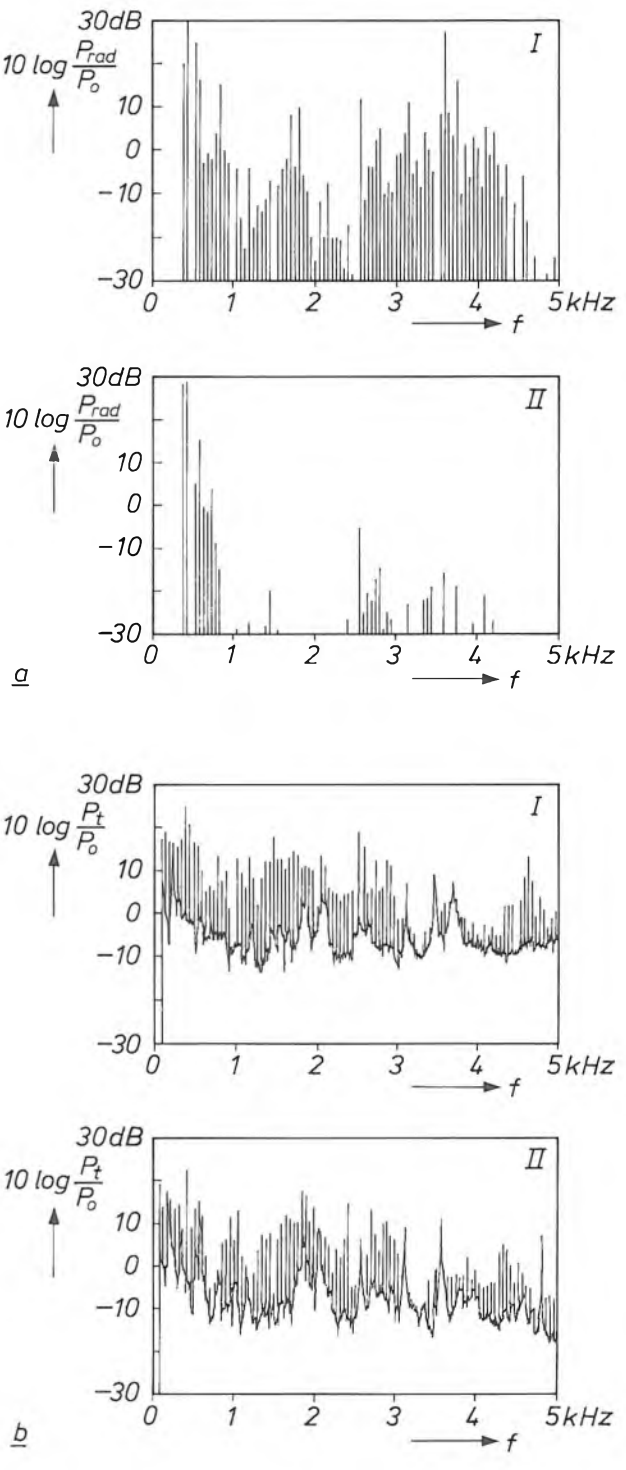

Fig. 13. *a*) Calculated power P_{rad} of the intake noise in dB ($P_0 = 10^{-12}$ W) as a function of frequency f for silencers *I* and *II*. *b*) The total measured noise power P_t of the compressor in dB, also for silencers *I* and *II*.

[9] L. J. M. Kuypers, G. A. A. Asselman and G. van den Berkmortel, Reed valve simulation: a comparison of numerical and experimental results, Proc. 15th Int. Congr. on Refrigeration, part 2, Venice 1979, pp. 795-801.

described. The three quantities that determine the power P_{rad} of the intake noise as a function of frequency f in equation (7) are thus available. $P_{rad}(f)$ is found by multiplying the three spectra for IL_d^{-1}, IL_b^{-1} and P_s. A program that also calculates a Fourier transform of the volume flow $q(t)$ as given by eq. (9) performs this multiplication fairly easily.

Fig. 13a shows the results of calculations for the compressor with intake silencer *I* and for the compressor with intake silencer *II*. Here again, the considerable improvement achieved by modifying the silencer can be seen. Fig. 13*b* shows the measured power spectra of the total noise produced by the compressor unit. The calculated and measured spectra for silencer *I* in particular demonstrate that the intake noise is an important part of the total noise output. The two spectra for silencer *II* differ more than the spectra for silencer *I* because the other noise sources become more significant when the silencer has been improved.

It also appears from the agreement between the calculated and measured spectra for silencer *I* that the models give a fairly good approximation of the behaviour of practical devices. The models can therefore be used for further improvements in the design of the intake silencer, and for reliable predictions in the future design of other kinds of reactive silencer.

Summary. Acoustic noise generated by a source inside an electrical appliance reaches the environment after the successive steps of excitation, transmission and radiation. Noise reduction can be achieved by tackling each of these steps separately. In a washing machine the motor is one of the main sources of noise. Measurements show that this noise originates mainly in the periodic abrupt change in the motor current from the thyristor-controlled power supply. A different power-supply circuit, improved motor supports and a soundproofed cabinet have reduced the noise from the washing machine by 5 dB(A) during the wash cycle. In the compressor unit of a refrigerator the main noise source is the intermittent intake of the Freon gas through the inlet valve. Calculations based on models have given a better understanding of the origin and transmission of this noise. Measurements show that the models correspond well to the behaviour of practical devices. Modifying the reactive intake silencer of the compressor unit gives a noise reduction of 3 dB(A).

Scientific publications

These publications are contributed by staff from the laboratories and other establishments that form part of or are associated with the Philips group of companies. Many of the articles originate from the research laboratories named below. The publications are listed alphabetically by journal title.

Philips GmbH Forschungslaboratorium Aachen, Weißhausstraße, 5100 Aachen, Germany — *A*

Philips Research Laboratory, Brussels, 2 avenue Van Becelaere, 1170 Brussels, Belgium — *B*

Philips Natuurkundig Laboratorium, Postbus 80000, 5600 JA Eindhoven, The Netherlands — *E*

Philips GmbH Forschungslaboratorium Hamburg, Vogt-Kölln-Straße 30, 2000 Hamburg 54, Germany — *H*

Laboratoires d'Electronique et de Physique Appliquée, 3 avenue Descartes, 94450 Limeil-Brévannes, France — *L*

Philips Laboratories, N.A.P.C., 345 Scarborough Road, Briarcliff Manor, N.Y. 10510, U.S.A. — *N*

Philips Research Laboratories, Cross Oak Lane, Redhill, Surrey RH1 5HA, England — *R*

Philips Research Laboratories, Sunnyvale, P.O. Box 9052, Sunnyvale, CA 94086, U.S.A. — *S*

K. Murata (*Univ. Osaka*) & D. F. Kyser *S*	Monte Carlo methods and microlithography simulation for electron and X-ray beams	Adv. Electron. & Electron Phys. **69**	175-259	1987
F. Weling & H. Wehr *A*	Properties of multiple clad fibers: experiments and numerical predictors	Appl. Opt. **26**	4852-4856	1987
B. A. Joyce, J. Zhang (*Imperial College of Sci. & Technol., South Kensington*), J. H. Neave & P. J. Dobson *R*	The application of RHEED intensity effects to interrupted growth and interface formation during MBE growth of GaAs/(Al,Ga)As structures	Appl. Phys. A **45**	255-260	1988
D. E. Lacklison, G. Duggan, J. J. Harris, C. T. B. Foxon, D. Hilton, C. Roberts & C. M. Hellon *R*	Slope resistance characteristics of GaAs-(Al,Ga)As-GaAs single barrier structures	Appl. Phys. Lett. **52**	305-307	1988
R. Pandya & A. Martinez *N*	Large-area defect-free silicon-on-insulator films by zone-melt recrystallization	*ibid.*	901-903	1988
K. Shahzad, D. J. Olego & D. A. Cammack *N*	Thickness dependence of strains in strained-layer superlattices	*ibid.*	1416-1418	1988
G. Frens & J. J. F. G. Heuts *E*	The double layer potential ϕ_δ as a rate determining factor in the coagulation of electrocratic colloids	Colloids & Surf. **30**	295-305	1988
P. C. M. Gubbens*, A. M. van der Kraan* (**Interuniv. Reactor Inst., Delft*) & K. H. J. Buschow *E*	$RFe_{10}V_2$ compounds studied by ^{57}Fe, ^{161}Dy, ^{166}Er and ^{169}Tm Mössbauer spectroscopy	Hyperfine Interactions **40**	389-392	1988
B. Gabillard, T. Ducourant, C. Rocher, M. Prost & J. Maluenda *L*	A 200-mW GaAs 1K SRAM with 2-ns cycle time	IEEE J. **SC-22**	693-698	1987
O. Boser & V. Newsome *N*	High frequency behavior of ceramic multilayer capacitors	IEEE Trans. **CHMT-10**	437-439	1987
W. J. van Gils *E*	Two-dimensional dot codes for product identification	IEEE Trans. **IT-33**	620-631	1986
E. Persoon *E*	A pipelined image analysis system using custom integrated circuits	IEEE Trans. **PAMI-10**	110-116	1988
G. Lütteke (*Philips Apparatefabrik, Krefeld*) & H. C. Raets *A*	220-V mains 500-kHz class-E converter using a BIMOS	IEEE Trans. **PE-2**	186-193	1987
P. Ruterana, J. P. Chevalier (*C.E.C.M.-C.N.R.S., Vitry*), P. Friedel & N. Bonnet (*Univ. Paris-Sud*) *L*	Cleaning and nitridation of (100) GaAs surfaces: a high resolution electron microscopy study	Inst. Phys. Conf. Ser. No. 87	27-32	1987
C. Schiller, M. Duseaux & J. P. Farges *L*	High resolution X-ray diffraction on GaAs and InP substrates	*ibid.*	621-626	1987

C. Dierieck	*B*	Pressure potential formulation of 2-D stokes problems in multiply-connected domains	Int. J. Numer. Methods in Fluids **7**	69-85	1987
R. Waser	*A*	Solubility of hydrogen defects in doped and undoped $BaTiO_3$	J. Am. Ceram. Soc. **71**	58-63	1988
P. Suchet, M. Duseaux, G. Gillardin, J. Le Bris & G. M. Martin	*L*	Evidence of the origin of infrared scattering in GaAs with high-resolution infrared tomography	J. Appl. Phys. **62**	3700-3703	1987
P. F. Fewster & C. J. Curling	*R*	Composition and lattice-mismatch measurement of thin semiconductor layers by X-ray diffraction	*ibid.*	4154-4158	1987
J. Petruzzello, B. L. Greenberg, D. A. Cammack & R. Dalby	*N*	Structural properties of the ZnSe/GaAs system grown by molecular-beam epitaxy	J. Appl. Phys. **63**	2299-2303	1988
R. N. Bhargava	*N*	Electronic states and pair emission in ZnSe	J. Lumin. **40 & 41**	24-27	1988
B. A. Joyce	*R*	Molecular beam epitaxy: recent trends and future developments	J. Phys. & Chem. Solids **49**	237-242	1988
A. Raymond*, R. Piotrzkowski*, J. L. Robert*, S. Azema* (**Univ. Montpellier*), M. Kubisa+, W. Zadwadzki+, L. Litwin-Staszewska+ (+*Univ. Warsaw*) & J. P. André	*L*	Impurities in GaAlAs-GaAs heterojunctions metastable character of Si states and magnetodonors	J. Phys. Colloq. **48**, Suppl. No. 11	C5/243-C5/246	1987
E. K. Broadbent	*S*	Nucleation and growth of chemically vapor deposited tungsten on various substrate materials: a review	J. Vac. Sci. & Technol. B **5**	1661-1666	1987
J. M. Towner	*S*	The importance of the short-circuit failure mode in aluminium electromigration	*ibid.*	1696-1700	1987
J.-P. Charlier & P. Van Dooren	*B*	On Kogbetliantz's SVD algorithm in the presence of clusters	Linear Algebra & Appl. **95**	135-160	1987
M. Iost, S. Gourrier, B. Bru, P. Rabinzohn & F. Pasqualini	*L*	Linewidth control in deep UV contact lithography	Microelectron. Eng. **6**	69-75	1987
M. Lemonier & C. Piaget	*L*	Solid state image sensors for electronic readout of image tubes	Onde Electr. **67**, No. 6 (November)	99-107	1987
J. A. Clarke	*R*	Current trends in optics for projection TV	Opt. Eng. **27**	16-22	1988
P. A. Devijver & M. M. Dekesel	*B*	Learning the parameters of a hidden Markov random field image model: a simple example	Pattern Recognition Theory and Applications, P. A. Devijver & J. Kittler (eds), NATO ASI Series, Vol. F30, Springer, Berlin Heidelberg	141-163	1987
J. Ayers & J. Ladell	*N*	Spectral widths of the Cu $K\alpha$ lines	Phys. Rev. A **37**	2404-2407	1988
D. J. Olego, K. Shahzad*, J. Petruzzello & D. Cammack	*N*	Depth profiling of elastic strains in lattice-mismatched semiconductor heterostructures and strained-layer superlattices	Phys. Rev. B **36**	7674-7677	1987
M. A. Fisher*, A. R. Adams*, E. P. O'Reilly* (**Univ. Surrey*) & J. J. Harris	*R*	Resonant electron scattering due to the central cells of impurities observed in AlGaAs under hydrostatic pressure	Phys. Rev. Lett. **59**	2341-2344	1987
F. Berz	*R*	Effect of barrier thickness on the quantum mechanical transmission across parabolic barriers	Phys. Stat. Sol. b **145**	K27-K30	1988
P. A. Devijver	*B*	Segmentation of binary images using third-order Markov mesh image models	Proc. 8th Int. Conf. on Pattern recognition, Paris 1986	259-261	1986
S. Mukherjee, M. Amato, I. Wacyk & V. Rumennik	*N*	LDMOS and LIGT's in CMOS technology for power integrated circuits	Proc. IEDM '87, Washington D.C., 1987	778-781	1987
P. Houdy, V. Bodart, C. Hily, P. Ruterana, L. Nevot (*Inst. d'Optique, Orsay*), M. Arbaoui* N. Alehyane* & R. Barchewitz* (**Univ. Pierre et Marie Curie, Paris*)	*L*	Performances of C-W multilayers as soft X-rays optics: high reflectivity in the range 2d = 60 to 100 Å	Proc. SPIE **733**	389-397	1987
M. Rocchi	*L*	GaAs digital IC's for computer applications	VLSI '87, C. H. Séquin (ed.), Elsevier Science, Amsterdam	221-234	1988

H. J. de Wit and K. Jager, Magnetic domains in amorphous alloys for tape-recorder heads,
Philips Tech. Rev. **44**, No. 4, 101-109, Sept. 1988.

Certain amorphous cobalt-containing alloys with high saturation polarizations (about 1 T) show promise for applications in tape-recorder heads for video recording at high information densities. The relative permeability μ_r, which has to be very high ($\mu_r \gtrsim 1000$) for reproducing the stored information, is largely determined by the structure of the magnetic domains. This can be controlled by annealing the alloys in a magnetic field, thus inducing a magnetic anisotropy. The effect on the permeability and the other magnetic properties depends on the direction of the magnetic field and the temperature during annealing, on the form of the material — spun ribbon or sputtered thin film — and on the precise composition.

E. W. Meijer, Polyepoxides; formation and properties of their network structure,
Philips Tech. Rev. **44**, No. 4, 110-121, Sept. 1988.

The polymerization of epoxide monomers with catalysts or initiators results in polyepoxides. Special attention is given to chain polymerization from bisepoxides: the three-dimensional networks formed permit a wide variety of applications. Methods of gaining a fundamental understanding of the formation of these networks and their structure are illustrated by two examples. In the first example it is shown how phosphorescence spectroscopy can be used to monitor changes in the molecular mobility of polymer segments, both during the formation of the network and as a function of temperature. In the second example it is shown how nuclear-magnetic-resonance spectroscopy can be used to study the mechanism of network formation with the aid of model compounds. Emphasis is placed here on the part played by the $Al(acac)_3$/catechol initiator-catalyst system.

J. Crucq, Theory and practice of acoustic noise control in electrical appliances,
PhilipsTech.Rev.**44**,No.4,123-134,Sept.1988.

Acoustic noise generated by a source inside an electrical appliance reaches the environment after the successive steps of excitation, transmission and radiation. Noise reduction can be achieved by tackling each of these steps separately. In a washing machine the motor is one of the main sources of noise. Measurements show that this noise originates mainly in the periodic abrupt change in the motor current from the thyristor-controlled power supply. A different power-supply circuit, improved motor supports and a sound-proofed cabinet have reduced the noise from the washing machine by 5 dB(A) during the wash cycle. In the compressor unit of a refrigerator the main noise source is the intermittent intake of the Freon gas through the inlet valve. Calculations based on models have given a better understanding of the origin and transmission of this noise. Measurements show that the models correspond well to the behaviour of practical devices. Modifying the reactive intake silencer of the compressor unit gives a noise reduction of 3 dB(A).

Name

Initials

Title

Address

stamp

as

postcard

Administration Department
Philips Technical Review

Philips Research Laboratories
Building WY 136

P.O. Box 80 000

5600 JA Eindhoven
The Netherlands

OTHER PHILIPS PUBLICATIONS

Philips Journal of Research

An English-language journal with articles on research at the various Philips Laboratories. Six issues per volume.
Information: Philips Journal of Research, Philips Research Laboratories, P.O. Box 80 000, 5600 JA Eindhoven.

Acta Electronica

An annual publication with a special subject for each year, with articles in French and English on electronics and applied physics.
Information: Acta Electronica, Laboratoires d'Electronique et de Physique appliquée, 3 Avenue Descartes, 94451 Limeil-Brévannes Cedex, France.

Philips Telecommunication and Data Systems Review

An English-language journal, dealing with developments, systems, and products in business communications, computers, computer networks, telecommunications services, radio communications and dictation equipment. Four issues per volume.
Information: Philips Telecommunication and Data Systems Review, P.O. Box 32, 1200 JD Hilversum, The Netherlands.

Electronic Components and Applications

An English-language journal with articles dealing with electronic components and materials and their applications. Four issues per volume.
Information: Electronic Components and Applications, Philips Electronic Components and Materials Division, P.O. Box 218, 5600 MD Eindhoven, The Netherlands.

Medicamundi

An English-language journal with articles on radiology, isotope diagnosis and medical electronics. Three issues per volume.
Information: Medicamundi, Philips Nederland, Boschdijk 525, 5621 JG Eindhoven, The Netherlands.

Forthcoming issues of Philips Technical Review will include articles on:

Theory of the quantum well

Magnetic-recording heads

Philips Tech. Rev. Vol. 44, No. 4, Sept. 1988

Contents

PHILIPS TECHNICAL REVIEW
Philips Research Laboratories
P.O. Box 80000
5600 JA Eindhoven
The Netherlands

Subscription rate per volume	fl. 80.00 or U.S. $ 35.00
Student's subscription	fl. 32.00 or U.S. $ 14.00
Binder	fl. 10.00 or U.S. $ 4.00

Payment only after invoicing, please.

Printed in the Netherlands